PRINT® NANOPARTICLE PARAMETERS TO IMPROVE DOCETAXEL PK/PD

Kevin Chu

A dissertation submitted to the faculty of the University of North Carolina at Chapel Hill in partial fulfillment of the requirements for the degree of Doctor of Philosophy in the Division of Molecular Pharmaceutics in the UNC Eshelman School of Pharmacy

Chapel Hill
2013

Approved by

Joseph M. DeSimone

Michael Jay

Russ Mumper

William Zamboni

Andrew Wang

ABSTRACT

Kevin Chu: PRINT® nanoparticle parameters to improve docetaxel PK/PD
(under the direction of Professor Joseph M. DeSimone)

Nanomedicines currently approved for oncology improve certain properties of the reformulated small molecule, such as toxicity, but do not always enhance efficacy or pharmacokinetics. Further research to advance the understanding of how nanoparticle design can affect *in vivo* performance will aid in the rational design of nanomedicines. Particle Replication in Non-wetting Templates (PRINT®) is a particle fabrication technique capable of making precisely controlled formulations which allows for the systematic evaluation of single formulation variables. In this dissertation, three formulation variables were evaluated: particle size of non spherical particles, drug loading and release kinetics.

The findings of this research indicate that reduced particle size decreases particle accumulation in the liver, spleen and lungs while enhancing plasma and tumor exposure. Reducing the drug loading of the particles had a similar effect, potentially due to blockading the mononuclear phagocyte system (MPS). Decreasing the release rate of docetaxel from the particles also improved the plasma exposure in addition to improving the maximum tolerated dose of drug. The improved tolerability through use of a prodrug strategy allowed a higher dose of docetaxel to be delivered to achieve improved tumor growth inhibition. Controlling the released docetaxel concentration within the plasma may be a key parameter to improve the safety and therapeutic profile of docetaxel.

ACKNOWLEDGEMENTS

I would like to acknowledge those individuals who assisted with the work. Mathew Finniss conducted the synthetic work, and has been a great colleague who I had many insightful scientific discussions with and who has always lent a helping hand. Mark Walsh and Allison Schorzman developed methods for tissue analysis. Charlene Ross and her core have helped conduct many *in vivo* studies. Kevin Herlihy and Charlie Bowerman assisted on the roll to roll. Ashley Galloway from Liquidia Technologies has also provided advice on assessing particle stability and scaling up particle purification. Elizabeth Enlow laid the ground work for fabricating PLGA particles and PLGA docetaxel particles.

I have been fortunate to have many great mentors I would like to acknowledge. My adviser Joseph DeSimone has provided me guidance and continually challenged me and offered me new opportunities to grow as a scientist. William Zamboni and Andrew Wang have worked closely with me and have always given time to discuss the dissertation work. Russ Mumper and Michael Jay have taught me a lot from my laboratory rotations and have continued providing mentorship as part of the committee. Mary Napier and Chris Luft have always been extremely supportive with everything they do. Z Haroon has continually provided me with a lot of scientific guidance and has taught me many valuable life lessons.

Finally, I would like to acknowledge my parents Sam and Dina for their continued support in my pursuits.

TABLE OF CONTENTS

LIST OF TABLES

LIST OF FIGURES

LIST OF ABBREVIATIONS

80x320 nm – particle with diameter (d) = 80 nm; height (h) = 320 nm;

200x200 nm – particle with diameter (d) = 200 nm; height (h) = 200 nm;

AUC – area under the curve

DLS – dynamic light scattering

DMSO – dimethyl sulfoxide

HPLC – high performance liquid chromatography

IC_{50}– half maximal inhibitory concentration

I.V. – intravenous

kDa – kilodaltons (equivalent to 1,000 grams per mole)

PBS – phosphate buffered saline

PDI – polydispersity index

PEG – poly(ethylene glycol)

PET – poly(ethylene terephthalate)

PFPE – perfluoropolyether

PK – pharmacokinetics

PLGA – poly(lactic-co-glycolic acid)

PLLA – poly(L-lactic acid)

PRINT – particle replication in non-wetting templates

PVOH – poly(vinyl alcohol)

R2R – roll to roll fabrication

SEM – scanning electron microscopy

SKOV3 – human ovarian adenocarcinoma cell line

T_g – glass transition temperature

(w/w) – denotes a percentage expressed as weight per weight

CHAPTER 1: INTRODUCTION

1.1 Specific Aims and Background

There have been multiple nanoparticle formulations indicated for cancer that have been approved by the Food and Drug Administration (FDA) and many more are in clinical development. Though some nanoparticles have received FDA approval and demonstrated superiority in preclinical models, nanoparticles have not demonstrated improvement in overall survival against the free small molecule formulation in phase III trials [1,2]. The goal of this research is to evaluate nanoparticle design parameters to identify optimal nanoparticle characteristics to improve the pharmacokinetics, toxicity and efficacy of a model drug, docetaxel. The specific aims of the research are to:

1. Evaluate the effect of particle size of non spherical particles on docetaxel pharmacokinetics
2. Evaluate the effect of nanoparticle weight percent drug loading on the pharmacokinetics and efficacy of docetaxel
3. Evaluate the effect of release kinetics on the pharmacokinetics and efficacy of docetaxel prodrug

The goal of this research is to improve the understanding of commonly measured nanoparticle characteristics on *in vivo* performance. To accomplish this, particles were prepared by a top-down fabrication process known as Particle Replication in Non-wetting Templates (PRINT®). The PRINT technique utilizes molds with negative features of the desired size and shape particles that one desires to make. Using PRINT, single formulation

parameters can be altered to evaluate its effect on pharmacokinetics and efficacy because PRINT offers precise control particle size, shape and composition. There are many alternative methods to prepare nanoformulations and these processes are summarized in the following sections.

Multiple alternative formulations of taxanes have been prepared to avoid use of Cremophor EL as well as improve pharmacokinetics, decrease toxicity and improve efficacy. The only FDA approved nanoparticle formulation of a taxane is Abraxane®, which is a Cremophor EL free formulation that consists of paclitaxel protein-bound particles. The paclitaxel protein-bound particles are ~130 nanometers (nm) and dissociate into smaller albumin particles. Abraxane allows a higher dose of paclitaxel to be administered (260 mg/m^2 versus (v) 175 mg/m^2) and shorter infusion time than Taxol® (3 hours v 30 minutes) [2]. Additionally, Abraxane had an improved safety profile; patients receiving Abraxane had lower incidence of high grade neutropenia (9% v 22%) [2]. However, in a phase III trial patients with metastatic breast cancer receiving Abraxane at 50% higher paclitaxel dose than Taxol as a first line treatment did not have improved median survival [2]. Abraxane did not improve the pharmacokinetics of paclitaxel when compared to Taxol, in fact, Abraxane increased the clearance of paclitaxel (17700 v 10740 $mL/hr/m^2$). Abraxane allows 50% higher dose of paclitaxel than Taxol, but plasma exposure as measured by area under the curve is similar for both formulations [3]. Abraxane improves the safety and convenience of paclitaxel administration, but overall did not improve the pharmacokinetics and perhaps, therefore did not improve efficacy despite delivering a higher dose of paclitaxel. Abraxane is unlike other nanoformulations because it dissociates into albumin particles *in vivo* and thus may not rely on the EPR effect to accumulate in tumors.

Other taxane formulations, such as NK105 also eliminate the need for Cremophor EL, but also improve the pharmacokinetics of paclitaxel. NK105 is a micellar formulation of paclitaxel that uses diblock polymers of polyethylene glycol (PEG) and polyaspartic acid to form micelles of ~90 nm in diameter that encapsulate paclitaxel in the core of the particle. Compared to Taxol, NK105 decreased the clearance rate (408.6 v 10740 mL/hr/m^2) and volume of distribution (4527.1 v 58900 mL/m^2) of total paclitaxel within the system and also increased the plasma exposure in a phase I trial [3]. NK105 was further evaluated in a phase II trial; 56 patients with advanced gastric cancer received NK105 as second line treatment. Overall response rate was 25% and median overall survival was 14.4 months [4]. Based on the modest activity seen, NK105 was advanced to a phase III trial that is comparing progression free survival compared to patients receiving Taxol. At this time, tolerability of NK105 appeared to be similar to that of Taxol, but further studies will determine if NK105 improves paclitaxel's safety profile [4]. Micelles are advantageous because they are formed by self-assembly and do not require extensive input of mechanical energy to form particles. However, their stability *in vivo* is reliant upon the critical micellar concentration (CMC) of the diblock polymer. NK105 appears to be quite stable *in vivo* based on the large differentiation in the pharmacokinetics of paclitaxel when dosed as a micellar formulation.

Another taxane formulation that also improves the pharmacokinetics of Taxol is poliglumex, which is a biodegradable polymer drug conjugate of paclitaxel that is ~48,000 daltons [5]. The polymer backbone is Poly-L-glutamic acid and paclitaxel is conjugated to the backbone via an ester linkage sensitive to the enzyme cathepsin B [5]. Compared to the other taxane formulations, poliglumex offers controlled and triggered release of paclitaxel from the polymer backbone because drug release requires internalization of the conjugate

followed by cleavage of the linker by the lysosomal enzyme cathepsin B. In pharmacokinetics studies, the entire conjugate had a longer terminal elimination half life compared to free paclitaxel, but, only 1-2% of paclitaxel was released from the conjugate [6]. Poliglumex was evaluated in multiple phase III clinical trials, including one that compared poliglumex and docetaxel head to head as second-line treatment for non small cell lung cancer. Patients who received poliglumex had less high grade neutropenia and shorter infusion times than patients receiving docetaxel [7]. However, poliglumex did not increase the median survival of patients [7]. Survival benefit may be limited by lack of release of paclitaxel from the poliglumex conjugate. Subgroup analysis of the phase III clinical trials show that efficacy may be enhanced in women compared to men, suggesting that cathepsin B levels may be important in predicting efficacy [8].

Other biodegradable nanocarrier systems include Samyang's Genexol®-PM and Bind Biosciences' BIND-014. Genexol-PM is a 20-50 nm micellar formulation of paclitaxel that is formed using diblocks of poly(lactide) and poly(ethylene glycol). In preclinical studies, Genexol-PM had 1.5-times higher maximum tolerated dose compared to Taxol [9]. In a phase I clinical trial, the recommended dose for further study was 300 mg/m^2, also higher than the typical Taxol dose [10]. Interestingly, compared to the other alternative taxane formulations, Genexol-PM requires a 3 hour infusion time [10]. Similar to Abraxane, the pharmacokinetics of paclitaxel with Genexol-PM is not improved compared to Taxol. At a similar dose to Taxol, the terminal elimination half life of paclitaxel dosed as Genexol-PM is actually less than that of paclitaxel dosed as Taxol [10]. Thus, the main benefit of Genexol-PM appears to be the removal of Cremophor EL from the formulation. Samyang also prepared a similar micelle, but with docetaxel rather than paclitaxel. However, with

docetaxel, the maximum tolerated dose and safety profile was found to be similar to the clinical formulation Taxotere in preclinical models [11].

The most recent taxane formulation that has entered clinical development is BIND-014, which is formulated by a nanoemulsion process using a mixture of Poly(L-lactide) and a diblock of Poly(L-lactide)-Poly(ethylene glycol) to make particles ~100 nm in diameter [12]. Compared to the other taxane formulations, BIND-014 provides sustained release of docetaxel over days, which is dependent upon the polymer and molecular weight selected. In preclinical studies, slower drug release rate was found to decrease the clearance rate of docetaxel and increase the terminal elimination half life [12]. Compared to the other taxane formulations that have been approved or are in clinical development, BIND-014 may be the most promising due to its addition of targeting. BIND-014 has targeting ligands that target prostate-specific membrane antigen (PSMA), which has been demonstrated to increase the retention of nanoparticles in a xenograft tumor [13]. In a phase I trial, BIND-014 increased the plasma exposure of total docetaxel compared to Taxotere. However, patients receiving BIND-014 were dose limited by neutropenia and can only be dosed as high as 60 mg/m^2, which is lower than a typical Taxotere dose.

These taxane formulations vary in their compositions and also greatly in their pharmacokinetics and toxicity. Though removal of Cremophor EL appears to improve the tolerability of paclitaxel, BIND-014 and Samyang's docetaxel formulations did not appear to improve the tolerability of docetaxel. In addition, it remains to be established if a nanoformulation may enhance the efficacy of docetaxel.

Though there are no current docetaxel liposomal formulations in clinical development, liposomes are an important tool in drug delivery. Liposomes are self-

assembled unilamellar or multilamellar vesicles prepared from phospholipids and can be sized from sub-100nm to micron sized particles. Liposomes have been extensively studied to deliver chemotherapeutics. They can encapsulate both hydrophilic and hydrophobic drugs within the aqueous core or within the bilayer and are prepared from biocompatible lipids [14]. However, release of the drug is not as well controlled because drug release is dependent on the aqueous solubility of the drug and also the composition of the lipid bilayer. The attractiveness of liposomes for drug delivery are their long circulation half lives, which can be hours or even days, because of the addition poly(ethylene glycol) to the surface of the liposome [15].

There have been multiple liposomal drug formulations approved by the food and drug administration (FDA). Doxil™, a liposomal formulation of the anti-cancer agent doxorubicin, is approved for ovarian cancer, AIDS-related Kaposi's Sarcoma and multiple myeloma in the United States. The half-life of doxil is ~73.9 hours in humans, much longer than that of doxorubicin (<10 minutes) [1]. The encapsulation of doxorubicin into liposomes greatly decreases the volume of distribution and clearance of doxorubicin compared to the non liposomal formulation [16]. The prolonged elmination half life of doxorubicin and reduced distribution may enhance passive targeting to tumors and reduce side effects. In a phase III trial comparing Doxil to conventional doxorubicin for first-line treatment of metastatic breast cancer, less patients receiving Doxil experienced cardiotoxicity, while efficacy as measured by progression-free survival was similar [1].

Though liposomes are one of the few FDA approved nanoparticle drug carriers, they do have some disadvantages. Liposomes do not offer as precise size control as the PRINT process. Additionally, liposomes typically have short shelf-lives unless lyophilized and have

lower drug loading and depending on the loading method and the drug, low encapsulation efficiency [17]. Also, drug release from liposomes is not as well controlled as polymeric particles.

1.2 PRINT PLGA docetaxel NPs

PLGA docetaxel NPs of the feature size d = 200 nm; h = 200 nm have been previously developed and reported by Elizabeth Enlow with % loadings up to 40. To more easily conduct *in vivo* studies, the PRINT process was scaled from a discontinuous bench top process (illustrated in figure 1.1) to a continuous fabrication scheme, referred to as the roll to roll (R2R) using the instrument shown in figure 1.2.

1.2.1 General protocol

For bench top fabrication, a solution at 1 w/w% PLGA and 1 w/w% docetaxel in chloroform can be used to draw individual films on PET sheets in segments of 6" x 12" to be individually placed through heated nips with the mold. In the R2R process, a roll of PET is placed at position 1.1B and is placed through the heated nips (position 1.1E) and collected at position 1.1G. Likewise, a roll of thin mold is placed at position 1.1A and collected at position 1.1F. As the PET moves from 1.1B to 1.1G, solution is deposited using a syringe pump at position 1.1C immediately before a mayer rod (1.1D), which casts the solution into a wet film. The solvent is then evaporated by heat guns aimed at the PET to give a dry film of polymer and drug. The contents of the dry film are then filled into mold at position 1.1E and collected to position 1.1G.

After the mold is filled, the mold is moved to position 1.1A to transfer the particles from the mold to PET that will be coated with low molecular weight polyvinyl alcohol (PVOH). During the particle transfer process, the mold and the PVOH coated PET are

brought together at the heated nips and collected together at 1.1F or 1.1G. The mold is then peeled away from the PVOH coated PET to leave an array of particles on the PET. The PET is run through two rollers and water is added to dissolve the PVOH and release the particles into a solution for further purification and storage.

1.2.2 R2R Parameter Optimization

Once an appropriate process has been established by discontinuous bench top fabrication, the parameters are adapted to achieve continuous fabrication. During this optimization, important parameters to control are film thickness of the polymer drug film as well as temperature of the heated nips. Film thickness is controlled by the w/w% solids of the particle forming solution, mayer rod number as well as speed that the roll of PET is pulled from 1.1C to 1.1J.

Process optimization was started with the 80x320 nm using a mayer #3 (figure 1.3A and B) or mayer #5 (figure 1.3C and D). Particles were fabricated with either mayer rod at 3 different w/w% solutions of PLGA and 3 different speeds. Particles were then harvested and analyzed by DLS. In general, increased mayer number, w/w% solution and speed lead to increased particle size and PDI. However, for the 80x320 nm particles, 2 w/w% solution and a speed of 4-8 ft/min yielded particles with good particle size and PDI.

Likewise, the R2R process was optimized for the 200x200 nm particles (shown in figure 1.4). As with the 80x320 nm particles, increased w/w% solution and speed generally gave increased particle size and PDI. A 2 w/w% solution and mayer #3 was sufficient to make good particles at speeds 4-8 ft/min, with there being a slight increase in PDI at 8 ft/min.

With these initial parameters, further optimization was done with the 2 w/w% solution. A mayer #2 was used to further decrease film thickness to reduce raw material use.

Additionally, speeds were altered between 4-8 ft/min. Final R2R parameters for the 80x320 nm particles were 6-7 ft/min, 2 w/w% solution and mayer rod #2. Similarly, the 200x200 nm parameters were 6-7 ft/min, 2 w/w% solution and mayer rod #3. Figure 1.5 shows PLGA docetaxel particles fabricated with the final process parameters.

After particle fabrication was optimized, the 80x320 particles were evaluated for storage stability. After particle fabrication, particles were flash frozen and stored at -20°C or lyophilized and stored at 4°C. At set time points, particles were removed and thawed or reconstituted in sterile water and measured by DLS. Particles had good physical stability when frozen and stored for 3 months or lyophilized and then stored at 4°C for 6 months.

1.3 Tumor Delivery

Chemotherapy delivery to solid tumors requires drug molecules to cross the vascular endothelium, the interstitial space of the tumor and then into the cancer cell to its molecular target. The encapsulation or linkage of drug molecules into nanoparticles or macromolecules has been thought to selectively enhance tumor accumulation of drug because some tumors may exhibit leakiness to allow larger molecules to extravasate, where as normal endothelium normally only allows smaller molecules (few nanometers) to extravasate [18]. The reduced permeability of chemotherapeutics in a nanoparticle to cross normal endothelium has the potential to decrease toxicity to non cancerous organs. However, encapsulation of drugs into nanoparticles does not guarantee increased extravasation across the vasculature into solid tumors because of formidable barriers presented by the physiology of solid tumors.

1.3.1 Tumor Vasculature

The enhanced permeability and retention effect is hypothesized to increase tumor accumulation of macromolecules and nanoparticles, but solid tumors exhibit many

unfavorable characteristics for mass transport. Tumor vasculature is not well distributed in the tumor and is more tortuous compared to normal vasculature [18]. The increased tortuosity of the vasculature increases resistance to blood flow and lowers perfusion rates in tumors compared to normal tissue. Decreased perfusion rates decreases opportunity for nanoparticles to extravasate across the vasculature. Because of tumor vasculature heterogeneity, only the periphery of a tumor may be well vascularized leading a necrotic core that has low penetration of nanoparticles.

Direct measurement of human tumors has shown that the interstitial fluid pressure is elevated [19,20]. This hypertension in the tumor relative to the vasculature decreases convection of nanoparticles and impedes mass transport into the tumor. When interstitial fluid pressure is high, diffusion is the predominate mode of mass transport. Though vasculature in mouse xenograft tumors may have interendothelial junctions that may be as wide as a few micrometers in diameter [21], large particles have slow diffusion and will not have as deep tumor penetration compared to smaller nanoparticles or traditional chemotherapeutics and antibody therapies that are less than a few nanometers. Additionally, deep tumor penetration is inhibited by the interstitial matrix that is primarily composed of collagen and other elastic fibers [22].

1.3.2 Effect of particle size on tumor delivery

Particle size and molecule size have been demonstrated to affect the percent injected dose accumulated at the tumor in *in vivo* models. In early studies, F. Yuan et al. found that the upper size range for extravasation of liposomes is between 400 – 600 nm in LS174T xenograft tumors [23]. More recent studies have demonstrated that in a pancreatic cancer xenograft model, micelles with a mean diameter of 30 nm had the best tumor accumulation

compared to micelles with diameters of 50, 70 and 100 nm [24]. Additionally, in two different xenografts, particles with diameter of 20 and 50 nm had improved tumor accumulation compared to particles with diameter of 200 nm [25, 26]. Additionally, the 50 nm particles with camptothecin were much more efficacious compared to the 200 nm particles in a Lew Lung Cancer (LLC) xenograft model [26]. Improved tumor delivery will likely be enhanced by decreasing particle diameter.

Though many studies have been done with spherical particles, few studies have utilized rod shaped or high aspect ratio particles. Prior work within the lab has demonstrated that high aspect ratio particles are more readily internalized by cells *in vitro*, and thus may be more useful to improve targeting of particles to cancer cells once active targeting ligands are conjugated to the particle surface [27]. However, rod shaped particles of high aspect ratio prepared through the PRINT® process requires that one dimension of the particle be greater than 100 nm with the smaller dimension being 80 nm. Though the 80 nm dimension is within the preferred range for tumor accumulation, it is unknown how the longer dimension of the particle will affect tumor accumulation as well as particle clearance. It is hypothesized that the shorter dimension of a rod shaped particle will have more influence on particle biodistribution than the longer dimension. Filtration studies of a series of rod shaped particles with a diameter of 80 nm, and length of 180 to 5000 nm, demonstrated that all particles, regardless of particle length, could pass through 0.2 μm filters [28]. Particle rigidity was more of an influence in particle recovery after filtration than particle length. Thus, a particle with a diameter less than the diameter of the pore is likely to cross the pore, even though particle length may be greater than the pore size. A rod shaped particle with a

small diameter may allow for improved tumor accumulation of an encapsulated chemotherapeutic.

1.3.3 Effect of drug loading on tumor delivery

Drug loading, defined as the percent by weight a drug constitutes a formulation has not been studied for its effect on drug pharmacokinetics or efficacy. For a small molecule, high plasma concentration of drug drives drug distribution through a concentration gradient. An increase in the number particles injected by decreasing drug loading may also drive more particles to the tumor through leaky vasculature. Though number of particles accumulated at the tumor may be increased by increasing particle dose, decreased drug loading per particle may not actually increase the amount of drug delivered to the tumor. Thus, evaluating the effect of drug loading on drug pharmacokinetics and efficacy may yield valuable insight on how well drug loading should be controlled within a manufacturing process. Ideally, drug loading should be kept as constant, but process changes in both particle fabrication and purification during the development process may lead to differences in drug loading. Understanding if drug loading alters pharmacokinetics will help predict if different batches of drug loaded nanoparticles will be bioequivalent during the development process. Additionally, decreased drug loading may lead to greater accumulation within the tumor and may be a parameter that can be tuned to maximize efficacy.

1.3.4 Effect of drug release kinetics on tumor delivery

Sustained drug release of a chemotherapeutic from a particle may lead to improved efficacy as well as improved tolerability. Particulate delivery of a chemotherapeutic is hypothesized to improve its tumor accumulation; this may require that minimal drug is released when the particle is in plasma and drug is triggered to release at the site of the tumor

or slowly releases, so that the majority of the released drug within the body is at the site of the tumor. J. Hrkach et al. demonstrated that by reducing docetaxel's *in vitro* release rate, the plasma pharmacokinetics of the total docetaxel (encapsulated and released docetaxel) is improved as measured by terminal elimination half life and exposure by AUC [12]. However, the influence of *in vitro* release rate on efficacy and toxicity was not evaluated. J. Hrkach et al. advanced its most stable formulation with the slowest *in vitro* release kinetics to a phase I trial. Though it appears that sustained release may lead to an increased duration that tumor cells are exposed to docetaxel, it is not known what release rate is optimal. Too slow of a release rate may improve tolerability, but decrease efficacy, if a minimum effective concentration of the chemotherapeutic is not reached. A quick release rate may release the majority of drug into plasma allowing for distribution into normal tissues. Evaluating the effect of release kinetics on efficacy and toxicity may hone in on an optimal release kinetic for chemotherapeutic delivery.

1.3 REFERENCES

[1] M.E.R. O'Brien, N. Wigler, M. Inbar, R. Rosso, E. Grischke, A. Santoro, et al. Reduced cardiotoxicity and comparable efficacy in a phase III trial of pegylated liposomal doxorubicin HCl (CAELYX/Doxil) versus conventional doxorubicin for first-line treatment of metastatic breast cancer. Ann Oncol 2004; 15: 440-9.

[2] W.J. Gradishar, S. Tjulandin, N. Davidson, H. Shaw, N. Desai, P. Bhar, et al. Phase III trial of nanoparticle albumin-bound paclitaxel compared with polyethylated castor oil-based paclitaxel in women with breast cancer. J Clin Oncol 2005; 23: 7794-803.

[3] T. Hamaguchi, K. Kato, H. Yasui, C. Morizane, M. Ikeda, H. Ueno, et al. A phase I and pharmacokinetic study of NK105, a paclitaxel-incorporating micellar nanoparticle formulation. Br J Cancer 2007; 97: 170-6.

[4] K. Kato, K. Chin, T. Yoshikawa, K. Yamaguchi, Y. Tsuji, T. Esaki, et al. Phase II study of NK105, a paclitaxel-incorporating micellar nanoparticle, for previously treated advanced or recurrent gastric cancer. Invest New Drugs 2012; 30: 1621-7.

[5] T. Hamaguchi, Y. Matsumura, M. Suzuki, K. Shimizu, R. Goda, I. Nakamura, et al. NK105, a paclitaxel-incorporating micellar nanoparticle formulation, can extend in vivo antitumour activity and reduce the neurotoxicity of paclitaxel. Br J Cancer 2005; 92: 1240-6.

[6] A.V. Boddy, E.R. Plummer, R. Todd, J. Sludden, M. Griffin, L. Robson, et al. A phase I and pharmacokinetic study of paclitaxel poliglumex (XYOTAX), investigating both 3-weekly and 2-weekly schedules. Clin Cancer Res 2005; 11: 7834-40.

[7] L. Paz-Ares, H. Ross, M. O'Brien, a Riviere, U. Gatzemeier, J. Von Pawel, et al. Phase III trial comparing paclitaxel poliglumex vs docetaxel in the second-line treatment of non-small-cell lung cancer. Br J Cancer 2008; 98: 1608-13.

[8] S.D. Chipman, F.B. Oldham, G. Pezzoni, J.W. Singer. Biological and clinical characterization of paclitaxel poliglumex (PPX, CT-2103), a macromolecular polymer-drug conjugate. Int J Nanomedicine 2006; 1: 375-83.

[9] S.C. Kim, D.W. Kim, Y.H. Shim, J.S. Bang, H.S. Oh, S. Wan Kim, et al. In vivo evaluation of polymeric micellar paclitaxel formulation: toxicity and efficacy. J Control Release 2001; 72: 191-202.

[10] T.-Y. Kim, D.-W. Kim, J.-Y. Chung, S.G. Shin, S.-C. Kim, D.S. Heo, et al. Phase I and pharmacokinetic study of Genexol-PM, a cremophor-free, polymeric micelle-formulated paclitaxel, in patients with advanced malignancies. Clin Cancer Res 2004; 10: 3708-16.

[11] S.-W. Lee, M.-H. Yun, S.W. Jeong, C.-H. In, J.-Y. Kim, M.-H. Seo, et al. Development of docetaxel-loaded intravenous formulation, Nanoxel-PM™ using polymer-based delivery system. J Control Release 2011; 155: 262-71.

[12] J. Hrkach, D. Von Hoff, M. Mukkaram Ali, E. Andrianova, J. Auer, T. Campbell, et al. Preclinical development and clinical translation of a PSMA-targeted docetaxel nanoparticle with a differentiated pharmacological profile. Sci Transl Med 2012; 4: 128ra39.

[13] F. Gu, L. Zhang, B. a Teply, N. Mann, A. Wang, A.F. Radovic-Moreno, et al. Precise engineering of targeted nanoparticles by using self-assembled biointegrated block copolymers. Proc Natl Acad Sci USA 2008; 105: 2586-91.

[14] M. Gulati, M. Grover, S. Singh, M. Singh. Lipophilic drug derivatives in liposomes. Int J Pharm 1998; 165: 129-68.

[15] A.L Kilbanov, K. Maruyama, V.P. Torchilin, L. Huang. Amphipathic polyethyleneglycols effectively prolong the circulation time of liposomes. FEBS Lett 1990; 268: 235-37.

[16] Doxil® (doxorubicin HCl liposome injection) Product Information

[17] A. Sharma, U.S. Sharma. Liposomes in drug delivery: Progress and Limitations. Int J Pharm 1997; 154: 123-40.

[18] H. Maeda, J. Wu, T. Sawa, Y. Matsumura, K. Hori. Tumor vascular permeability and the EPR effect in macromolecular therapeutics: a review. J Control Release 2000; 65: 271-84.

[19] R.K. Jain. Transport of molecules across tumor vasculature. Cancer Metastasis Rev 1987; 6: 559-93.

[20] Y. Boucher, J.M. Kirkwood, D. Opacic, M. Desantis, R.K. Jain. Interstitial hypertension in superficial metastatic melanomas in humans. Cancer Res 1991; 51: 6691-94.

[21] H. Hashizume, P. Baluk, S. Morikawa, J.W. McLean, G. Thurston, S. Roberge et al. Openings between defective endothelial cells explain tumor vessel leakiness. Am J Pathol 2000; 156: 1363-80.

[22] R.K. Jain. Transport of molecules in the tumor interstitum; a review. Cancer Res 1987; 47: 3039-51.

[23] F. Yuan, M. Dellian, D. Fukumura, M. Leunig, D.A. Berk et al. Vascular Permeability in a Human Tumor Xenograft: Molecular Size Dependence and Cutoff Size. Cancer Res 1995; 55: 3752-56.

[24] H. Cabral, Y. Matsumoto, K. Mizuno, Q. Chen, M. Murakami et al. Accumulation of sub-100 nm polymeric micelles in poorly permeable tumors depends on size. Nat Nanotechnol 2011; 12: 815-23.

[25] L. Tang, N.P. Gabrielson, F.M. Uckun, T.M. Fan, J. Cheng. Size-dependent tumor penetration and in vivo efficacy of monodisperse drug-silica nanoconjugates. Mol Pharm 2013; 10: 883-92.

[26] L. Tang, T.M. Fan, L.B. Borst, J. Cheng. Synthesis and biological response of size-specific, monodisperse drug-silica nanoconjugates. ACS Nano 2012; 6: 3954-66.

[27] S.E. Gratton, P.A. Ropp, P.D. Pohlhaus, J.C. Luft, V.J Madden. The effect of particle design on cellular internalization pathways. Proc Natl Acad Sci USA 2008; 105: 11613-18.

[28] F.R. Kersey, T.J. Merkel, J.L. Perry, M.E. Napier, J.M. DeSimone. Effect of aspect ratio and deformability on nanoparticle extravasation through nanopores. Langmuir 2012; 28: 8773-81.

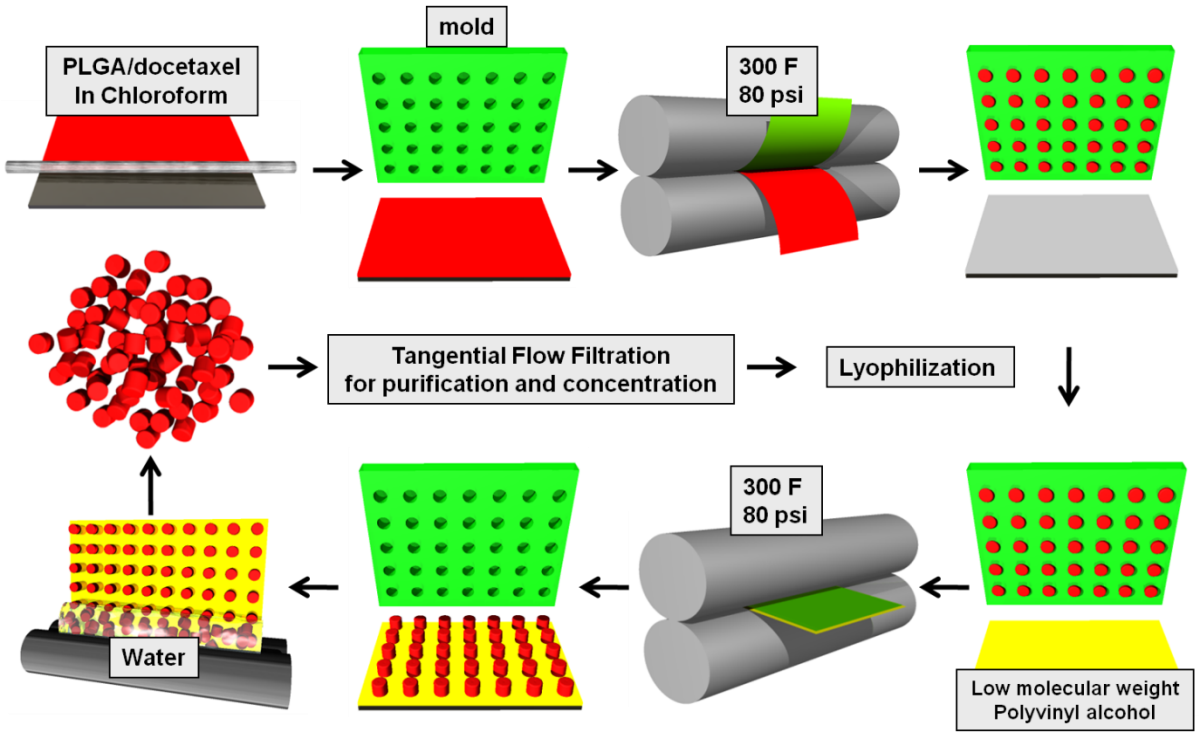

Figure 1.1. Discontinuous fabrication scheme of PRINT PLGA docetaxel NPs (Figure provided by Elizabeth Enlow)

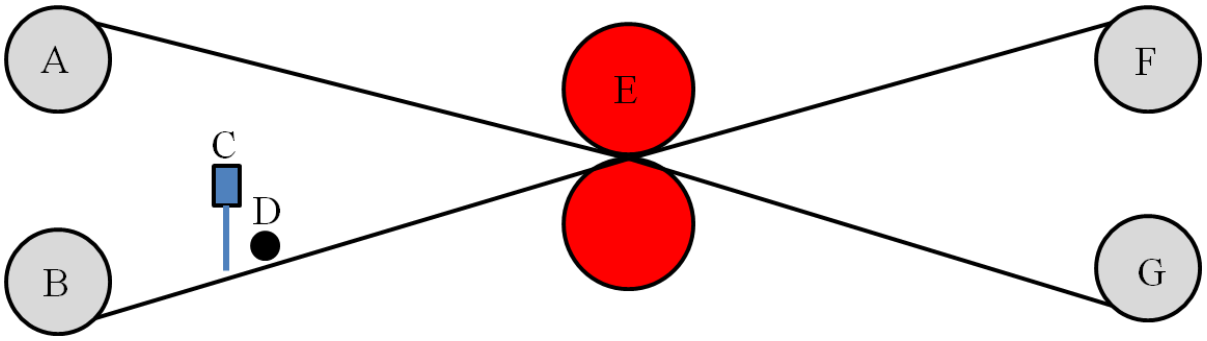

Figure 1.2. Roll to Roll (R2) continuous fabrication of PRINT particles

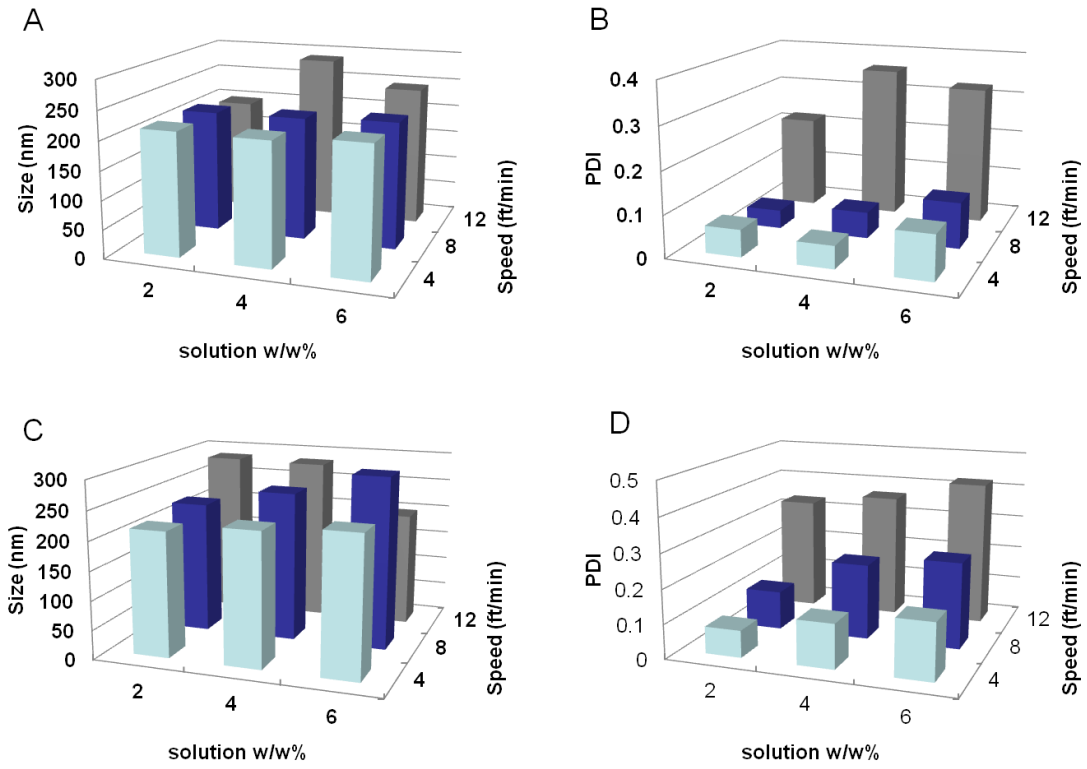

Figure 1.3. R2R optimization of 80x320 nm PLGA particles. A and B used a mayer rod #3. C and D used a mayer rod #5.

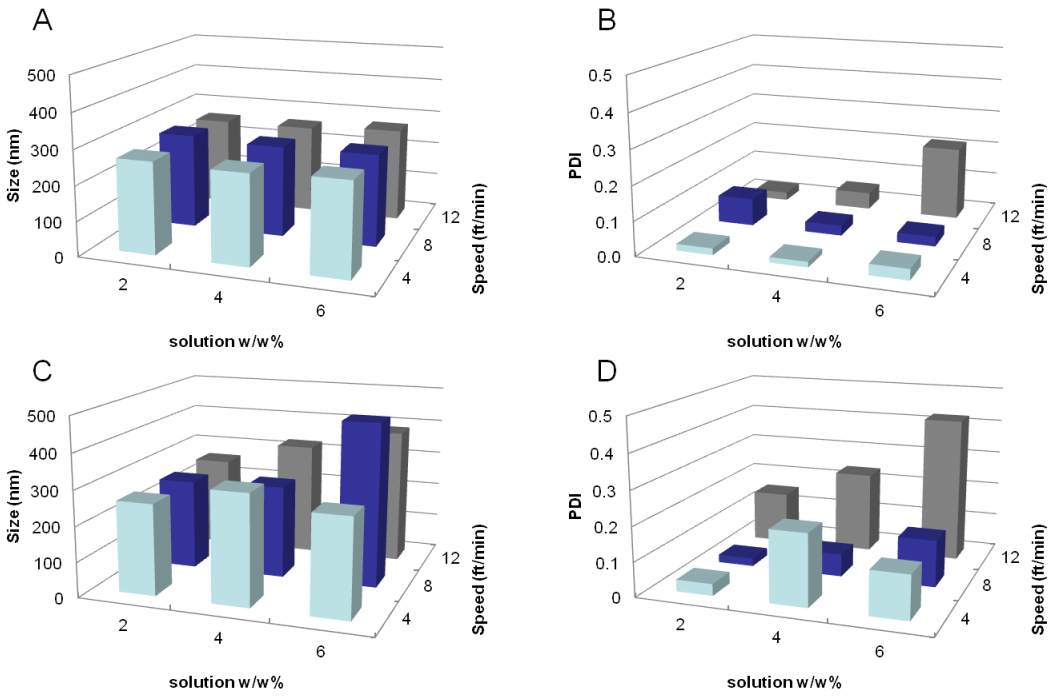

Figure 1.4. R2R optimization of 200x200 nm PLGA particles. A and B used a mayer rod #3. C and D used a mayer rod #5.

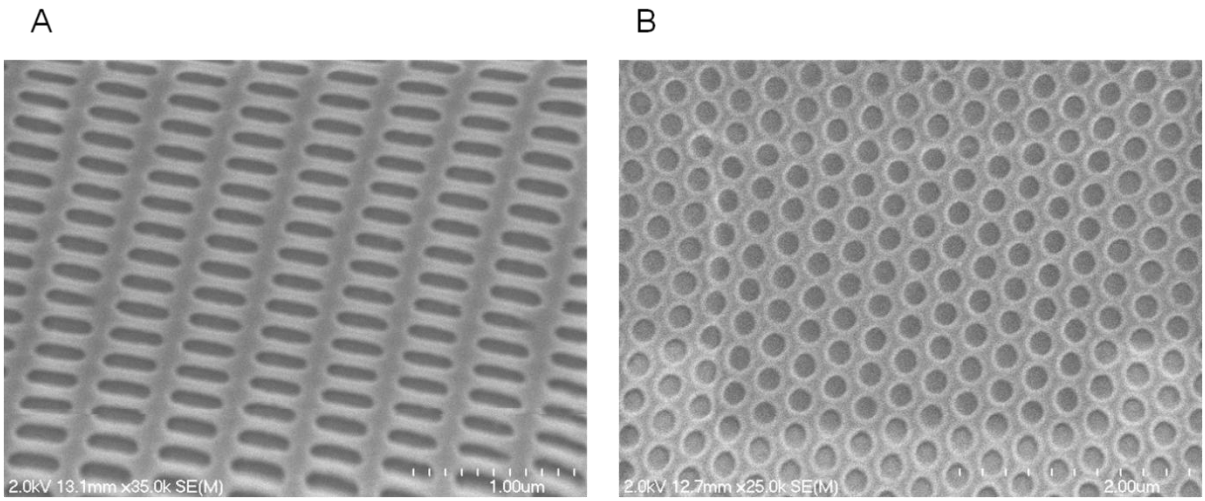

Figure 1.5. SEM of (A) 80x320 and (B) 200x200

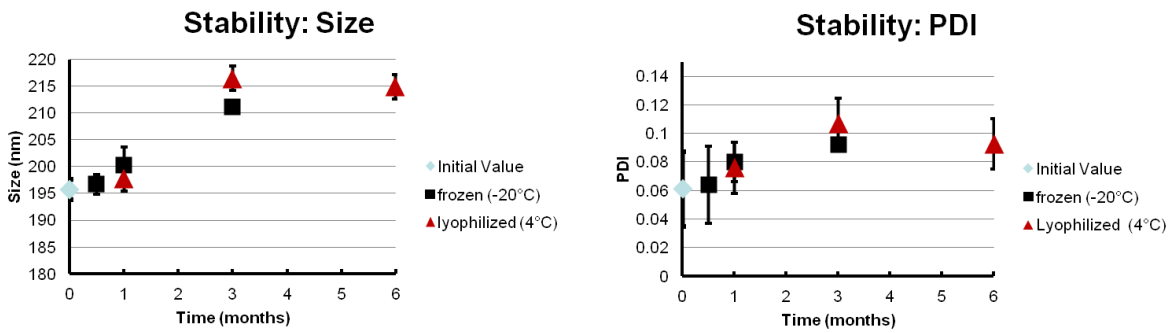

Figure 1.6. 80x320 PLGA docetaxel particles stored at -20°C after being flash frozen or stored at 4°C after being lyophilized.

CHAPTER 2: PLASMA, TUMOR AND TISSUE PHARMACOKINETICS OF DOCETAXEL DELIVERED VIA NANOPARTICLES OF DIFFERENT SIZES AND SHAPES IN MICE BEARING SKOV-3 HUMAN OVARIAN CARCINOMA XENOGRAFT

2.1 Introduction

The application of nanotechnology to oncology explores the use of macromolecular and nanoparticle carriers to enhance delivery of therapeutics and diagnostic agents. Desired outcomes of nanoparticle delivery include enhanced apparent drug solubility, extended drug half-life, and passive targeting to solid tumors by the enhanced permeability and retention (EPR) effect [1,2] all of which may translate to improved efficacy and decreased toxicity. Two Food and Drug Administration (FDA) approved examples of nanoparticle formulations are Doxil® (pegylated liposomal doxorubicin) and Abraxane® (albumin-bound paclitaxel nanoparticle). Doxil's advantages compared to doxorubicin are increased half-life of doxorubicin in plasma and great tumor delivery and also reduced cardiotoxicity that was demonstrated in a single agent phase III study [3]. Abraxane showed benefit in response rate and progression free survival in a single agent phase III trial compared to Taxol [4]. Though there has been success in nanomedicine, the percent of injected dose of nanoparticles that reaches the tumor remains low, and thus further study of factors affecting nanoparticle tumor accumulation are warranted [5].

There are many formulation techniques for nanoparticle fabrication, including self-assembled systems such as microemulsions [6] and micelles [7], liposomes [8],

emulsion/solvent evaporation [9] and nanoprecipitation [10] based polymeric particles. Particle compositions and fabrication techniques may vary, but nanoparticles for small molecule chemotherapy delivery have similar design criteria [11–13]. Nanoparticles are typically sized larger than 10 nm to avoid renal clearance and extravasation to normal tissues and are smaller than 200 nm to reduce clearance by the liver and spleen of the mononuclear phagocyte system (MPS) [14,15]. Although general trends have been established in desired particle size for tumor accumulation and there have been some studies on the role of particle size and shape on cellular uptake of particles [16–18], few studies have explored the effect of particle shape on *in vivo* tumor accumulation. Geng *et al* demonstrated that flexible filomicelles have longer plasma circulation times and evade the MPS [19]. Chauhan *et al* have demonstrated that a rod shaped particle with a small diameter has better tumor penetration than spherical particles of similar hydrodynamic diameter [20].

However, to date, the interdependent effect of size and shape on chemotherapeutic tumor delivery has not been explored. In this study, we applied the PRINT® (Particle Replication In Non wetting Templates) technology, which is a soft-lithography process, to fabricate monodisperse populations of PLGA particles with high loadings of Docetaxel [21]. PRINT is a top-down fabrication technique that produces size and shape specific particles that provides the ability to understand the role of size and shape on particle distribution *in vivo* [22]. Two particle shapes were used; diameter (d) = 200 nm; height (h) = 200 nm (200x200); and d = 80 nm; h = 320 nm (80x320); cylindrical particles. The 80x320 particle has an aspect ratio of 4:1. Though this particle has a longer length than the 200x200 particle, the 80 nm diameter may allow the particle to transport through smaller pores. With both particle shapes, we demonstrated improved plasma pharmacokinetics and tumor delivery

compared to the approved clinical formulation of Taxotere. Additionally, differences in clearance can be seen for the two PRINT particles suggesting that shape may play a role in reducing clearance by the MPS and enhancing tumor delivery.

2. 2 Methods

2.2.1 Materials

Poly(D,L-lactide-co-glycolide) (lactide:glycolide 85:15, 0.65 dL/g Inherent Viscosity at 30ºC) was purchased from Sigma-Aldrich. Chloroform and solvents (acetonitrile and water) for high performance liquid chromatography (HPLC) were purchased from Fisher Scientific. Docetaxel was purchased from LC Laboratories. Taxotere (free docetaxel) was purchased from the University of North Carolina at Chapel Hill hospital pharmacy for research purposes. Poly(ethylene terephthalate) (PET) sheets (6" width) were purchased from KRS plastics. Fluorocur®, 200x200 and 80x320 prefabricated molds and 2,000 g/mol polyvinyl alcohol (PVOH) coated PET sheets were provided by Liquidia Technologies.

2.2.2 Particle Fabrication

Docetaxel particles were fabricated following previously published methods with modification [23]. A thin film of PLGA and docetaxel was deposited on a 6"x12" sheet of PET by spreading 150µL of a 10 mg/mL PLGA and 10 mg/mL docetaxel chloroform solution using a # 5 Mayer Rod (R.D. Specialties). The solvent was evaporated with heat. The PET sheet with the film was then placed in contact with the patterned side of a mold and passed through heated nips (ChemInstruments Hot Roll Laminator) at 130ºC and 80psi. The mold was split from the PET sheet as they both passed through the hot laminator. The patterned side of the mold was then placed in contact with a sheet of PET sheet coated with 2,000 g/mol PVOH. This was then passed through the hot laminator to transfer the particles

from the mold to the PET sheet. The mold was then peeled from the PET sheet. The particles were removed by passing the PVOH coated PET sheet through motorized rollers and applying water to dissolve the PVOH to release the particles. To remove excess PVOH, the particles were purified and then concentrated by tangential flow filtration (Spectrum Labs).

2.2.3 Particle Characterization

Particles were imaged by scanning electron microscopy (SEM) by pipetting a 50 µL sample of particle on a glass slide. The sample was then dried and coated with 3 nm gold palladium alloy using a Cressington 108 auto sputter coater. Images were taken at an accelerating voltage of 2 kV using a Hitachi model S-4700 SEM. For size and zeta potential measurement, dynamic light scattering (DLS) (Malvern Instruments Nano-ZS) was used.

2.2.4 Drug Loading

Docetaxel was measured using an Agilent Technologies Series 1200 HPLC with a C18 reverse phase column (Zorbax Eclipse XDB-C18, 4.6x150mm, 5 micron). A linear gradient from 100% water to 100% acetonitrile was run over 10 minutes. Then 100% acetonitrile was run for 5 minutes. The flow rate was 1 mL/min and detection was at 210nm. Particle samples were prepared by diluting the sample 1 in 10 with acetonitrile and mixing the sample to break down the particle. Standards of docetaxel and PLGA were prepared in acetonitrile.

2.2.5 *In Vitro* Release Studies

100 µL of particle solution (200 µg/mL docetaxel) was placed in a mini dialysis unit with a 20k MW cutoff and dialyzed against a stirred 1L bath of 1xPBS at 37ºC. The bath was replaced periodically to maintain sink conditions. There were three dialysis units for

each time point. At each time point, the particle solution in each dialysis unit was removed and centrifuged to pellet the nanoparticles. The pellet was then analyzed for the amount docetaxel remaining. To determine the percent docetaxel released over time, the amount docetaxel remaining was compared to the initial amount of docetaxel in the system.

2.2.6 SKOV-3 human ovarian carcinoma tumor xenografts

This study was done with an approved protocol with the University of North Carolina at Chapel Hill's Institutional Animal Care and Use Committee. All animals used were treated humanely. SKOV-3 human ovarian carcinoma cells, acquired from ATCC, were propagated in culture and harvested in log-phase growth. Female C.B.-17 SCID mice, aged 6-8 weeks and 14-18 grams in body weight, were ordered from Harlan Sprague Dawley. The mice were acclimated for 1 week prior to tumor cell injection. Cells (5.0×10^6 cells in 200µL 1xPBS) were injected subcutaneously (SC) into the right flank of each mouse. Tumor volume was calculated using the formula: tumor volume (mm^3) = $(w^2 \times l)/2$, where w = width and l = length in mm of the tumor.

2.2.7 Pharmacokinetic study

42 days after tumor cell implantation, mice were pair matched according to tumor volume into three treatment groups. Individual tumor volumes ranged from 40 to 253 mm^3 at the time of grouping. The dosage for Docetaxel administered was based upon previously published work [24]. All mice received 10 mg/kg docetaxel via a single tail vein injection. Group 1 (n = 17) received free docetaxel. Group 2 (n = 18) received 200x200. Group 3 (n = 18) received 80x320. Formulations were diluted to 1 mg/mL of docetaxel with normal saline and mice were dosed at 10 µL of solution per gram of body weight.

Mice (n=3 per time point) were sacrificed at 0.083, 1, 6, 24, 72, and 168 hours after dosing. Blood (~1 mL) was collected via terminal cardiac puncture using sodium heparin as an anticoagulant under CO_2 anesthesia and processed for plasma by centrifugation (1,500 × *g* for 5 min). Plasma and tissues were placed in cryopreservation vials and preserved by snap freezing using liquid nitrogen. Tissues were stored at -80°C until analysis. Samples were processed for sum total (encapsulated + released) docetaxel using a protein precipitation method and analyzed by LC-MS/MS.

2.2.8 Sample Preparation and Processing

Total tissue and tumor weight was recorded at time of collection. Whole tissue and tumors were snap frozen in liquid nitrogen and stored at -80°C until homogenized. To form homogenates, the intact tissues or tumors were thawed and sectioned. The sections were weighed and diluted in a 1:3 ratio with phosphate buffered saline (PBS) solution (assumes tumor and tissue has a density of 1 mg/ml). Finally, these mixtures were homogenized by placing zirconium oxide beads (15 small and 2 large) into 2 mL tubes at 3,000 x *g* using a Precellys 24 homogenizer (Bertin Technologies) twice for 15 sec each with a 5 sec wait between each run. The resulting homogenates were snap frozen in liquid nitrogen and stored at - 80°C until processed.

Sample processing for determining plasma, tissue, or tumor concentrations of docetaxel was similar and based on previously published methods [25]. Calibration standards, quality control samples, and dilution control samples were prepared in equivalent matrix that had demonstrated no interfering components by the addition of 10 µl of a 10X solution of analyte in acidified methanol (0.1%v/v acetic acid). Dilution controls and diluted unknown samples were diluted 1:10 (10 uL sample + 90 uL appropriate matrix) prior to any

processing. All samples, standards, and controls were processed as follows: 100µl of plasma or, tumor or tissue homogenate was pipetted into a 96-well silanized glass insert, protein-precipitated with the addition of 100 µl of a 50:50 mixture of methanol:acetonitrile containing the internal standard solution (paclitaxel), vortexed for 1 min, and centrifuged for 15 min at 3,000 x g at 4ºC. The supernatants were analyzed by liquid chromatography with detection by tandem mass spectrometry with no further manipulation needed.

2.2.9 Liquid Chromatography Tandem Mass Spectrometry (LC-MS/MS)

A previously described LC-MS/MS analytical method was used for the quantification of analytes [26]. A Shimadzu solvent delivery system, and an Applied Biosystems API 4000 triple quadruple mass spectrometer with an APCI ion source (Applied Biosystems) were used for these analytical studies. Separation was accomplished using a Gemini® C18, 30x2.0 mm column, with a 5 µm particle size. The mass spectrometer was operated in positive ion mode using multiple reaction monitoring: docetaxel, 808.5→527.5 *m/z* and paclitaxel 854.4→286.1 *m/z* [26].

2.2.10 Pharmacokinetic Analysis

The pharmacokinetics of free docetaxel, 200x200 and 80x320 in plasma, tumor and tissue were analyzed by noncompartmental methods using WinNonlin Professional Edition version 5.2.1 (Pharsight Corp, Cary, NC). The area under the concentration versus time curve (AUC) was calculated using the linear up/log down rule. AUC from 0 to t (AUC_{0-t}) and AUC from 0 to ∞ ($AUC_{0-\infty}$) were calculated. Volume of distribution (V_d) and clearance (CL) were calculated using standard equations. The maximum concentration (C_{max}), time of C_{max} (T_{max}), last measured concentration (C_{last}) and time of C_{last} (T_{last}) were determined by visual inspection of the concentration versus time curve data.

2.2.11 Statistics

Data was analyzed for statistical differences by one-way analysis of variance (ANOVA) followed by Bonferroni's modified t-test for multiple comparisons using GraphPad Prism (GraphPad Software, Inc., La Jolla, CA). The confidence interval was set at 95% ($P<0.05$) to determine statistical significance.

2.3 Results

2.3.1 Particle Fabrication

The characteristics for the 80x320 and 200x200 particles are shown in **Table 2.1**. The PRINT fabrication process makes highly monodisperse particles as visualized by the SEM images (**Figure 2.1**). The particles had slightly negative zeta potential because of the PVOH that remains associated with the particle following harvesting and purification and because the PLGA was ester terminated. During fabrication, the particles are transferred from the mold to PVOH coated PET sheets. When the harvest sheet is dissolved with water during bead harvesting to release the particles from the sheet to solution, PVOH is adsorbed onto the particle surface. This slightly negative zeta potential may decrease nonspecific cellular uptake.

Particles were measured for size by DLS. Although the non-spherical particle shapes are not ideal for DLS measurement, the recorded measurements for both particle shapes were greater than 200 nm and the difference in hydrodynamic diameter was only ~30 nm. The similarity of hydrodynamic diameter allows for a more fair comparison of shape effects on drug pharmacokinetics.

Additionally, as previously demonstrated [23], the docetaxel w/w% is much higher than what can currently be achieved with conventional bottom up formulation approaches

[27–30]. The 80x320 particles were loaded at a lower w/w% than the 200x200 particles (33.5% vs 45.2%) due to the purification process post particle fabrication. The particles were originally charged with 50% by weight of docetaxel. Particles were washed with sterile water and concentrated by tangential flow filtration, which allowed some docetaxel to leach. The 80x320 loses a larger percentage of docetaxel during this purification process. This observation also matches the *in vitro* release profile of docetaxel from the particles (**Figure 2.2**). The 80x320 particles have a greater burst release than the 200x200 particles. ~60% of the docetaxel is released *in vitro* for 80x320 particles by 3 hours compared to ~38% for the 200x200 particles. Additionally, at 24 hours, nearly 100% of drug is released from the 80x320 particles mean while the 200x200 particles still hold ~27% of its cargo. The difference in release may be dictated by the particle geometry. Per unit volume, a 80x320 particle has more surface area compared to a 200x200 particle. This calculation assumes the 80x320 particle is a cylinder that is 80 nm in diameter and has a length of 320 nm and assumes the 200x200 particle is a cylinder that is 200 nm in diameter and has a length of 200 nm. Increased surface area per unit volume leads to faster drug release.

2.3.2 Pharmacokinetics of PRINT particles and free docetaxel

Sum total (encapsulated and released) docetaxel was measured for each organ. The concentration versus time profiles of Taxotere, 200x200 and 80x320 in plasma, tumor, spleen, liver and lungs are presented in **Figure 2.3**. The pharmacokinetic parameters of free docetaxel, 200x200 and 80x320 in plasma, tumor, spleen, liver and lungs are presented in **Table 2.2**. The PRINT particles had ~20-fold higher plasma exposure as measured by AUC compared to free docetaxel. The 80x320 and 200x200 particles had ~5-fold and ~7-fold higher maximal plasma docetaxel concentration than free docetaxel, respectively. The

difference in C_{max} was statistically significant higher for both PRINT particles compared to free docetaxel ($P<0.05$). Additionally, the volume of distribution was much lower for the PRINT particles compared to free docetaxel. The V_d for 80x320 and 200x200 was ~18-fold and ~33-fold, respectively, less than that of free docetaxel. Encapsulation of docetaxel into PRINT particles also decreased the clearance by ~24-fold compared to free docetaxel.

The 80x320 and 200x200 particles had a 53% and 76% increase in total tumor docetaxel exposure compared to free docetaxel from 0 to 168 h. Interestingly, looking at the tumor concentration versus time curve for 0 to 24 hours, the 80x320 particles gave a higher docetaxel exposure than the 200x200 particles, despite 200x200 particles having higher exposure from 0-168 hours. The tumor $AUC_{0\text{-}24h}$ for 80x320 was 20% higher than 200x200, but for $AUC_{0\text{-}168}$, the value for 200x200 particles was ~15.5% higher than that of 80x320. Also, the maximal tumor docetaxel concentration was at 1 hour for the 200x200 particles as opposed to 6 hours for the 80x320 particles. Additionally, the docetaxel concentration at 24 hours was higher for the 80x320nm particles compared to the 200x200nm particles (387 ng/mL versus 27 ng/mL). This indicates that the 80x320 may have steady accumulation at the site of the tumor. The plasma AUC for 0-24 hours and 0-168 hours of the 80x320 and 200x200 particles are similar. Thus, for the same plasma exposure from 0-24 hours, it appears that the 80x320 is more efficient at delivering docetaxel to the tumor than the 200x200 particle. However, from 0-168 hours, for similar plasma exposure, the 200x200 gave higher docetaxel exposure in the tumor. The C_{last} of the 200x200 particles was higher in the tumor than the 80x320 particles. Changing the 80x320 particle to decrease drug release rate may increase docetaxel exposure at the tumor at longer time points.

Both particles had higher docetaxel exposure in the spleen and liver compared to free docetaxel as expected for a nanoparticle formulation [5,12-13]. However, the 200x200 particles had ~4.8-fold higher docetaxel exposure in the spleen compared to the 80x320 particles. The maximal spleen concentration was also higher for the 200x200 particles compared to 80x320 (18,038 ng/mL vs 32,333 ng/mL, statistically significant). The spleen docetaxel concentration for the 200x200nm particles was also higher than the 80x320nm particles at all times points after 5 minutes. Despite the longer 320nm dimension, the higher aspect ratio 80x320 particle had less docetaxel exposure in the spleen compared to the 200x200 particles.

The liver docetaxel exposure for the 200x200 particle was 1.4-fold higher than 80x320 particles for $AUC_{0\text{-}24h}$. However, the maximal concentrations were not significantly different. The lung docetaxel exposure for the 200x200 particle was also 1.4-fold higher than 80x320 particles. The 200x200 particles also gave a higher maximal docetaxel concentration in the lungs compared to the 80x320 particles, which was statistically significant. The 200x200 particles, possible due to its larger diameter, gets cleared more in organs such as the lung, liver and spleen compared to the 80x320 particles.

2.4 Discussion

Monodisperse size and shape specific PLGA docetaxel nanoparticles were fabricated by the PRINT process. These particles had very high loadings of docetaxel relative to other nanoparticles of docetaxel [27-30]. Although the role of drug loading on drug pharmacokinetics and efficacy has not yet been established, higher drug loaded particles allows for less of the non-active excipients to be injected. The formulations Taxotere and Taxol may cause adverse reactions related to the surfactants used (polyoxyethylated castor

oil and tween 80) [31,32]. Thus, injecting less non active excipient relative to active drug may increase tolerability of the formulation, especially as related to infusion related reactions [4, 33].

The PRINT particles resulted in much higher plasma exposures of docetaxel compared to free docetaxel. Accordingly, the volume of distribution and clearance of the PRINT particles was reduced related to free docetaxel. Encapsulation of docetaxel into PRINT nanoparticles keeps the docteaxel more confined to the plasma compartment to allow for longer circulation and subsequently increased tumor accumulation. Additionally, reduced distribution to normal tissues may enhance the tolerability of the PRINT formulation compared to free docetaxel. Furthermore, the two particles had similar plasma docetaxel exposure, but from 0-24 hours, the 80x320 particle had higher tumor docetaxel exposure compared with 200x200. Thus, though different particles may have longer circulation times and higher plasma drug exposure, the shape of the particle may play a role in the efficiency of delivery to the tumor. Because minimal amount of drug compared to total dose administered reaches the tumor, incremental changes to improve tumor delivery and transport may prove to be worthwhile.

Shape selection may also aid in reducing nanoparticle clearance from MPS related organs such as the spleen and liver. Despite its longer 320 nm dimension, the 80x320 particle had reduced docetaxel exposure in the spleen, liver and lung than the 200x200 particle. Thus, the smallest dimension of the particle may be the determining factor of particle clearance and therefore drug clearance. On a similar note, Chauhan et al found that d = 14 nm; h = 55 nm rods had the same tumor transport as 13 nm PEG-coated CdSe/CdS quantum dots, and concluded that the smallest dimension may be the determining factor in

tumor transport [20]. Thus, future particle design may be dictated by choosing smaller particle diameters for better tumor delivery and MPS evasion.

However, though particles with smaller diameter may be preferred for enhanced passive targeting applications, smaller particles will typically have increased drug release rates due to increased surface to volume ratio. This likely explains the higher docetaxel levels for 80x320 particles in the tumor from 0-24 hours, but not from 0-168 hours compared to the 200x200 particles. Decreasing release rate may also be preferred to keep docetaxel within the particle while the majority of particles are still circulating within the first 24 hours after administration. Studies have been conducted to determine the effect of drug release rate on pharmacokinetics and biodistribution in particles of the same size that have varied release rate by using different polymers as well as a prodrug strategy.

Fabrication of particles by the PRINT produces monodisperse particles of specific size and shape that allows for the study of the effects of size and shape on drug distribution. In this study, the effect of size and shape on docetaxel pharmacokinetics was studied using a higher aspect ratio shaped 80x320 particle and a 200x200 particle. Both particles were compared to the clinical comparator for docetaxel, Taxotere. The 80x320 and 200x200 particles both resulted in much higher docetaxel plasma levels and also greatly decreased distribution volume and clearance. The increase in docetaxel plasma exposure due to docetaxel particle encapsulation led to increased tumor docetaxel exposure for both particles compared to free docetaxel. The 80x320 particle had higher tumor docetaxel accumulation from 0-24 hours and also higher docetaxel plasma levels than the 200x200 particles at24 hours. Additionally, the 80x320 particle had significantly less docetaxel exposure in the spleen as well as the liver and lungs. Though both particles had improved pharmacokinetics

over free docetaxel, the 80x320 particle may be preferred for long circulation due to its smaller diameter to penetrate pores, which results in better evasion of the MPS and higher tumor accumulation. Future studies that track particle biodistribution are being conducted to determine if the measured drug concentrations reported in this study follows the concentration – time trend of the particle itself.

2.5 REFERENCES

[1] Matsumura Y, Maeda H. A new concept for macromolecular therapeutics in cancer chemotherapy: mechanism of tumoritropic accumulation of proteins and the antitumor agent smancs. Cancer Res 1986; 46: 6387-92.

[2] Maeda H, Wu J, Sawa T, Matsumura Y, Hori K. Tumor vascular permeability and the EPR effect in macromolecular therapeutics: a review. J Control Release 2000; 65: 271-84.

[3] O'Brien MER. Reduced cardiotoxicity and comparable efficacy in a phase III trial of pegylated liposomal doxorubicin HCl (CAELYXTM/Doxil") versus conventional doxorubicin for first-line treatment of metastatic breast cancer. Ann Oncol 2004; 15: 440-449.

[4] Gradishar WJ, Tjulandin S, Davidson N, Shaw H, Desai N, Bhar P, et al. Phase III trial of nanoparticle albumin-bound paclitaxel compared with polyethylated castor oil-based paclitaxel in women with breast cancer., J Clin Oncol 2005; 23: 7794-803.

[5] Chrastina A, Massey KA, Schnitzer JE. Overcoming in vivo barriers to targeted nanodelivery. Wiley Interdiscip Rev Nanomed Nanobiotechnol 2011; 3: 421-37.

[6] Dong X, Mattingly CA, Tseng MT, Cho MJ, Liu Y, Adams VR, et al., Doxorubicin and paclitaxel-loaded lipid-based nanoparticles overcome multidrug resistance by inhibiting P-glycoprotein and depleting ATP. Cancer Res 2009; 69: 3918-26.

[7] Kim SC, Kim DW, Shim YH, Bang JS, Oh HS, Wan Kim S, et al. In vivo evaluation of polymeric micellar paclitaxel formulation: toxicity and efficacy. J Control Release 2001; 72: 191-202.

[8] Needham D, Anyarambhatla G, Kong G, Dewhirst MW. A new temperature-sensitive liposome for use with mild hyperthermia: characterization and testing in a human tumor xenograft model. Cancer Res 2000; 60: 1197-201.

[9] Doiron AL, Chu K, Ali A, Brannon-Peppas L. Preparation and initial characterization of biodegradable particles containing gadolinium-DTPA contrast agent for enhanced MRI., Proc Natl Acad Sci USA 2008; 105: 17232-7.

[10] Gu F, Zhang L, Teply BA, Mann N, Wang A, Radovic-Moreno AF, et al. Precise engineering of targeted nanoparticles by using self-assembled biointegrated block copolymers. Proc Natl Acad Sci USA 2008; 105: 2586-91.

[11] Farokhzad O, Langer RS. Nanoparticle Delivery of Cancer Drugs. Annu Rev Med 2011; 63: 185-198.

[12] Petros RA, DeSimone JM. Strategies in the design of nanoparticles for therapeutic applications. Nat Rev Drug Discov 2010; 9: 615-27.

[13] Yoo JW, Chambers E, Mitragotri S. Factors that control the circulation time of nanoparticles in blood: challenges, solutions and future prospects. Curr Pharm Des 2010; 16: 2298-307.

[14] Choi HS, Liu W, Misra P, Tanaka E, Zimmer JP, Itty Ipe B, et al. Renal clearance of quantum dots. Nat Biotechnol 2007; 25: 1165-70.

[15] Chen LT, Weiss L. The role of the sinus wall in the passage of erythrocytes through the spleen. Blood 1973; 41: 529-37.

[16] Champion JA, Mitragotri S. Shape induced inhibition of phagocytosis of polymer particles. Pharm Res 2009; 26: 244-9.

[17] Gratton SE, Ropp PA, Pohlhaus PD, Luft JC, Madden VJ, Napier ME, et al., The effect of particle design on cellular internalization pathways. Proc Natl Acad Sci USA 2008; 105: 11613-8.

[18] Sharma G, Valenta DT, Altman Y, Harvey S, Xie H, Mitragotri S, et al. Polymer particle shape independently influences binding and internalization by macrophages. J Control Release 2010; 147: 408-12.

[19] Geng Y, Dalhaimer P, Cai S, Tsai R, Tewari M, Minko T, et al. Shape effects of filaments versus spherical particles in flow and drug delivery. Nat Nanotechnol 2007; 2: 249-55.

[20] Chauhan VP, Popović Z, Chen O, Cui J, Fukumura D, Bawendi MG, et al. Fluorescent nanorods and nanospheres for real-time in vivo probing of nanoparticle shape-dependent tumor penetration. Angew Chem Int Ed Engl 2011; 50: 11417-20.

[21] Rolland JP, Maynor BW, Euliss LE, Exner AE, Denison GM, DeSimone JM, Direct fabrication and harvesting of monodisperse, shape-specific nanobiomaterials. J Am Chem Soc 2005; 127: 10096-100.

[22] Jeong W, Napier ME, DeSimone JM. Challenging nature's monopoly on the creation of well-defined nanoparticles, Nanomedicine (Lond) 2010; 5: 633-9.

[23] Enlow EM, Luft JC, Napier ME, DeSimone JM. Potent engineered PLGA nanoparticles by virtue of exceptionally high chemotherapeutic loadings. Nano Lett 2011; 11: 808-13.

[24] Zamboni WC, Strychor S, Joseph E, Parise RA, Egorin MJ, Eiseman JL. Tumor, tissue, and plasma pharmacokinetic studies and antitumor response studies of

Docetaxel in combination with 9-nitrocamptothecin in mice bearing SKOV-3 human ovarian xenografts. Cancer Chemother Pharmacol 2008; 62: 417-26.

[25] Hou W, Watters JW, McLeod HL. Simple and rapid Docetaxel assay in plasma by protein precipitation and high-performance liquid chromatography-tandem mass spectrometry. J Chromatogr B Analyt Technol Biomed Life Sci 2004; 804: 263-7.

[26] Zamboni WC, Combest AJ, DeLoia JA, Edwards RP, Bridges AS, Zamboni BA, et al. Pharmacologic and phenotypic study of Docetaxel in patients with ovarian or primary peritoneal cancer. Cancer Chemother Pharmacol 2011; 68: 1255-62.

[27] Cheng J, Teply BA, Sherifi I, Sung J, Luther G, Gu FX, et al. Formulation of functionalized PLGA-PEG nanoparticles for in vivo targeted drug delivery. Biomaterials 2007; 28: 869-76.

[28] Murugesan S, Ganesan S, Averineni RK, Nahar M, Mishra P, Jain NK. PEGylated Poly(Lactide-co-Glycolide) (PLGA) Nanoparticulate Delivery of Docetaxel: Synthesis of Diblock Copolymers, Optimization of Preparation Variables on Formulation Characteristics and In Vitro Release Studies. J Biomed Nanotechnol 2007; 3: 52-60.

[29] Musumeci T, Ventura CA, Giannone I, Ruozi B, Montenegro L, Pignatello R, et al. PLA/PLGA nanoparticles for sustained release of Docetaxel. Int J Pharm 2006; 325: 172-9.

[30] Senthilkumar M, Mishra P, Jain NK. Long circulating PEGylated poly(D,L-lactide-co-glycolide) nanoparticulate delivery of Docetaxel to solid tumors. J Drug Target 2008; 16: 424-35.

[31] Dye D, Watkins J, Suspected anaphylactic reaction to Cremophor EL. Br Med J 1980; 280: 1353.

[32] Kadoyama K, Kuwahara A, Yamamori M, Brown JB, Sakaeda T, Okuno Y. Hypersensitivity reactions to anticancer agents: data mining of the public version of the FDA adverse event reporting system, AERS. J Exp Clin Cancer Res 2011; 30: 93.

[33] ten Tije AJ, Verweij J, Loss WJ, Sparreboom A. Pharmacological effects of formulation vehicles: IMPLICATIONS for cancer therapy. Clin Pharmacokinet 2003; 42: 665-85.

Particle	Dtxl w/w%	Size (nm)	PDI	Zeta Potential (mV)
80x320	33.5	227 ± 10	0.18 ± 0.03	-3.2 ± 0.5
200x200	45.2	263 ± 1.8	0.09 ± 0.01	-3.4 ± 0.5

Table 2.1. Characterization of particles used in the pharmacokinetics study.

Specimen	Parameter	Units	Formulation		
			Free docetaxel	200x200	80x320
Plasma	AUC_{0-t}	ng/mL·h	5,809 (0-72h) 5,358 (0-24h)	138,359 (0-168h) 134,429 (0-72h) 136,942 (0-24h)	136,419 (0-168h) 133,462 (0-72h) 132,041 (0-24h)
	C_{max}	ng/mL(mean±SD)	*,†10,550±1,431	‡75,167±2,843	52,233±3,656
	CL	mL/h/kg	1,757	72	73
	V_d	mL/kg	8,509	257	474
Tumor	AUC_{0-t}	ng/mL·h	224,481(0-168h) 63,197 (0-24h)	396,104 (0-168h) 79644 (0-24h)	342,937 (0-168h) 95,516 (0-24h)
	C_{max}	ng/mL (mean±SD)	3,564±949	4,413±323	4,187±23
	T_{max}	h	1	1	6
	C_{last}	ng/mL	568	2321	757
	T_{last}	h	168	168	168
Liver	AUC_{0-t}	ng/mL·h	10,902 (0-24h)	264,273(0-168h) 87,255 (0-24h)	91,770 (0-168h) 64,274 (0-24h)
	C_{max}	ng/mL (mean±SD)	15,167±2,324	13,400±964	10,920+2,275
	C_{last}	ng/mL	19.4	682	16.3
	T_{last}	h	24	168	168
Spleen	AUC_{0-t}	ng/mL·h	13,298 (0-24h)	2,258,411 (0-168h) 712,579 (0-24h)	470,351 (0-168h) 324978 (0-24h)
	C_{max}	ng/mL (mean±SD)	*,†2,947±605	‡32,333±5,659	18,038±6,260
	C_{last}	ng/mL	59.6	4,106.3	67.8
	T_{last}	h	24	168	168
Lung	AUC_{0-t}	ng/mL·h	13,575 (0-72h)	62,791.9 (0-168h) 50,887 (0-72h)	44,377 (0-72h)
	C_{max}	ng/mL (mean±SD)	†4,070±590	‡7,280±225	4,967±709
	C_{last}	ng/mL	21.3	43.9	46.3
	T_{last}	h	72	168	72

Table 2.2. Pharmacokinetic parameters for free docetaxel, 200x200 and 80x320. * denotes statistical significance between free docetaxel and 80x320. † denotes statistical significance between free docetaxel and 200x200. ‡ denotes statistical significance between 80x320 and 200x200. $AUC_{0\text{-}t}$ is area under the curve from 0 to specified time. CL is clearance. V_d is volume of distribution. C_{max} is the maximal concentration and T_{max} is the time at which this occurred. C_{last} is the last measurable concentration and T_{last} is the time at which this occurred. All mice received 10 mg/kg docetaxel.

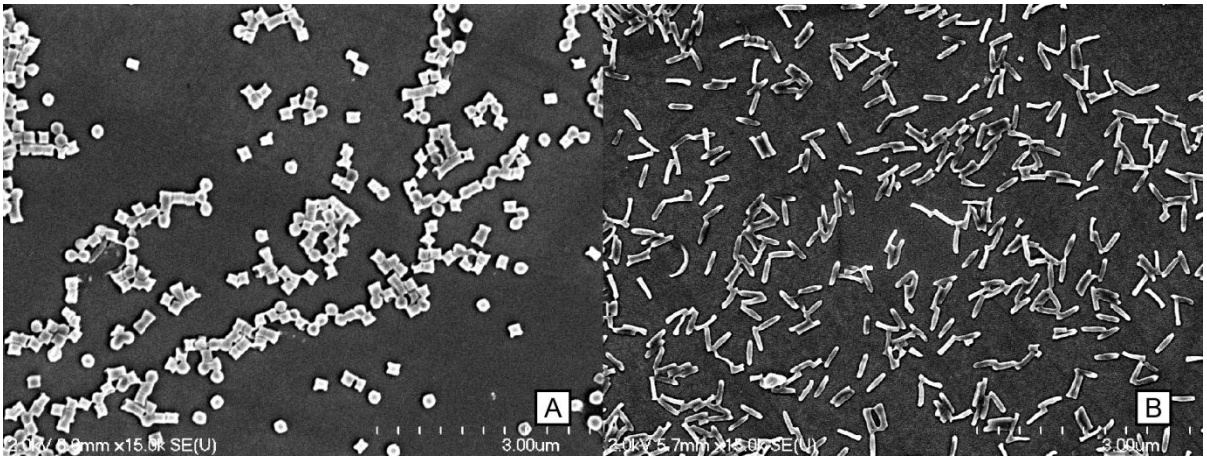

Figure 1. Scanning electron microscopy image of (A) 200x200 particles and (B) 80x320 particles

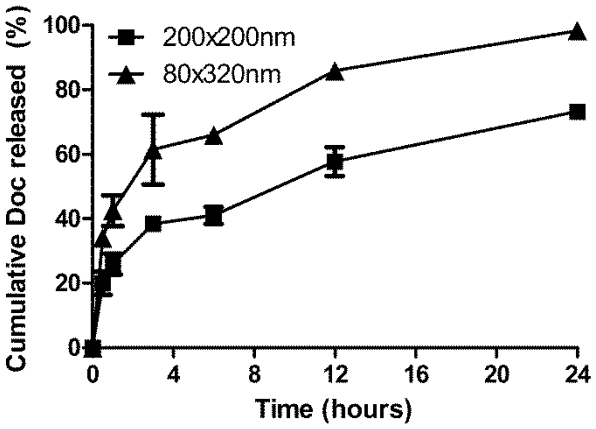

Figure 2.2. Percent Docetaxel released from 80x320 and 200x200 particles when incubated at 37ºC in 1xPBS. ■ for 200x200 particles and ▲ for 80x320 particles. N=3 measurements per time point.

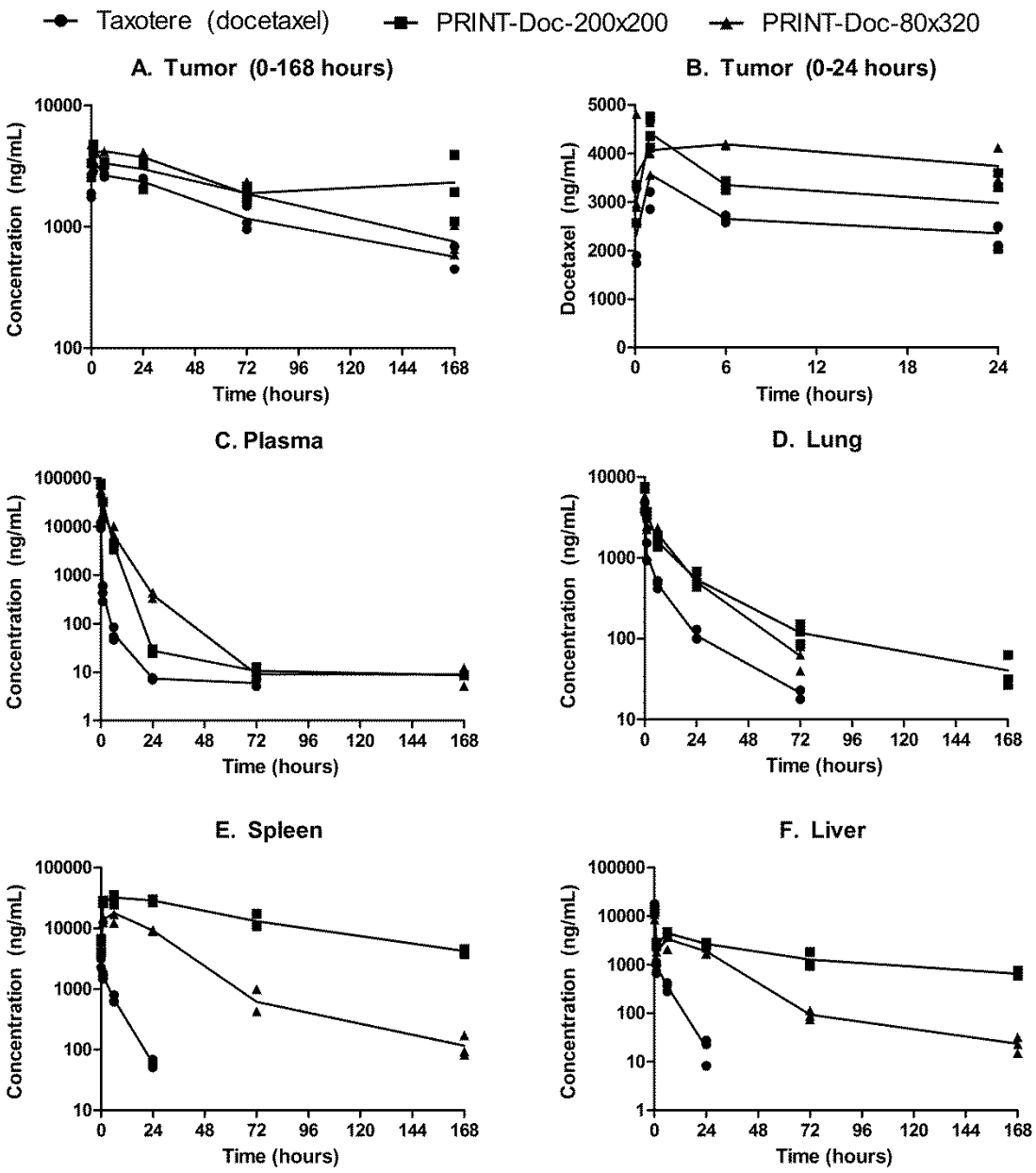

Figure 2.3. Docetaxel concentration versus time curve for (A) Tumor (0-168 hours), (B) Tumor (0-24 hours), (C) Plasma, (D) Lung, (E) Spleen and (F) Liver. Docetaxel concentration values for each mouse are represented by ● for free docetaxel, ■ for 200x200 particles and ▲ for 80x320 particles. The lines are connected by the mean value for each time point. Drug concentrations may not be shown for all time points if concentration detected was below the limit of detection. All mice received 10 mg/kg docetaxel.

CHAPTER 3: NANOPARTICLE DRUG LOADING AS A DESIGN PARAMETER TO IMPROVE DOCETAXEL PHARMACOKINETICS AND EFFICACY

3.1 Introduction

NP drug delivery has the potential to improve the effectiveness of small molecule chemotherapeutics. Though design parameters such as particle geometry [1–5] and surface chemistry [6] have been extensively studied to improve passive targeting, the effect of NP drug loading on therapeutic efficacy and pharmacokinetics has not been evaluated. NP drug loading is highly variable and often dependent upon the fabrication process. Polymeric formulations prepared by nanoprecipitation typically only achieve 1-2% drug loading, but NPs prepared by emulsion/solvent evaporation have reported drug loadings as high as 14% [7,8]. Other commonly used nanocarriers that encapsulate chemotherapeutics such as liposomes, microemulsions and micelles also only achieve ~10% drug loading [9–12].

To our knowledge, no prior studies have evaluated the relationship between drug loading in NPs and the pharmacokinetics and efficacy of small molecules *in vivo*. To fill this knowledge gap, we aimed to compare particles with two different drug loadings. To accomplish this, we prepared biodegradable NPs containing docetaxel using the soft-lithography template-based fabrication approach known as PRINT®. The PRINT® technology is capable of fabricating size and shape-specific particles with variable loadings of docetaxel [13]. In this report, the pharmacokinetics and efficacy of two identically sized and shaped NPs at 9% or 20% docetaxel loading were evaluated *in vivo*.

3.2 Materials and Methods

3.2.1 Materials

Poly(D,L-lactide-co-glycolide) (lactide:glycolide 85:15, 0.65 dL/g Inherent Viscosity at 30ºC) and Poly(L-lactide) (0.5 dL/g Inherent Viscosity at 25ºC) were purchased from Sigma-Aldrich. Chloroform and solvents (acetonitrile and water) for high performance liquid chromatography (HPLC) were purchased from Fisher Scientific. Docetaxel was purchased from LC Laboratories. Taxotere® (free docetaxel) was purchased from the University of North Carolina at Chapel Hill hospital pharmacy for research purposes. Poly(ethylene terephthalate) (PET) sheets (6" width) were purchased from KRS plastics. Fluorocur®, diameter (d) = 80 nm; height (h) = 320 nm; (80x320) prefabricated molds and 2,000 g/mol polyvinyl alcohol (PVOH) coated PET sheets were provided by Liquidia Technologies.

3.2.2 Particle Fabrication and Characterization

Particles were fabricated with solutions of PLA, PLGA and docetaxel dissolved in chloroform. The ratio of PLA:PLGA was 30:70. Two particle formulations at different weight percents of docetaxel were prepared. The particle fabrication and characterization follows previously published methods [13].

3.2.3 A549 human alveolar adenocarcinoma tumor xenografts

This study was done with an approved protocol with the University of North Carolina at Chapel Hill's Institutional Animal Care and Use Committee. All animals used were treated humanely. A549 cells were acquired from ATCC. Female nude mice, aged 4-6 weeks and ~20 grams in body weight, were ordered from University of North Carolina at Chapel Hill's animal core. The mice were acclimated for 1 week prior to tumor cell injection.

Cells (5.0×10^6 cells in 200 µL 1xPBS) were injected subcutaneously into the right flank of each mouse. Tumor volume was calculated using the formula: tumor volume (mm^3) = ($w^2 \times l$)/2, where w = width and l = length in mm of the tumor.

For the orthotopic lung cancer model, A549-luciferase-c8 cells were harvested and suspended in phosphate buffered saline and BD Matrigel Basement Membrane Matrix at a ratio of 4:1. Cells (5.0×10^6 cells in 50 µL 1xPBS:Matrigel) were injected directly into the left lung parenchyma [14].

3.2.4 Pharmacokinetic study

40 days after cells were inoculated subcutaneously when all mice had a median tumor volume of 150 mm^3, mice were pair matched according to tumor volume. All mice received 10 mg/kg docetaxel via a single tail vein injection. Formulations were diluted to 1 mg/mL of docetaxel with normal saline and mice were dosed at 10 µL of solution per gram of body weight. Mice (N=3 per time point per arm) were sacrificed at 0.083, 1, 6, 24, 72, and 168 hours after dosing. Blood (~1 mL) was collected via terminal cardiac puncture using K3-EDTA as an anticoagulant under CO_2 anesthesia and processed for plasma by centrifugation (1,500 × g for 5 min). Plasma and tissues were placed in cryopreservation vials and preserved by snap freezing using liquid nitrogen, and stored at -80°C until analysis. Tissues were homogenized in water (1:3, tissue:water) prior to analysis [15].

3.2.5 Protein precipitation

Docetaxel and paclitaxel stock solutions (1 mg/mL) were stored in methanol at -20°C. The standard curve concentrations of docetaxel in matrix were 1, 3, 5, 10, 30, 50, 100, 300, 500, 1000, 3000 and 5000 ng/mL and the quality control (QC) concentrations were 4, 40, 400, and 4000 ng/mL. The matrix for the standard curve and QCs consisted of control mouse

plasma for all plasma samples, or control plasma mixed 1:1 with a control tissue homogenate for the tissue being analyzed. A liver/plasma surrogate matrix was used for tumor samples. All tumor and tissue samples were mixed 1:1 with control plasma prior to analysis. Docetaxel was dissolved from the NP and extracted from 50 µL of sample by protein precipitation with 200 µL acetonitrile/0.1% formic acid containing 20 ng/mL paclitaxel internal standard. Samples were vortexed for 5 minutes and centrifuged at 3,000 x *g* for 10 minutes at 4°C. 170 µL supernatant was transferred to a clean 1.5 mL tube, lyophilized under nitrogen and reconstituted in 60 □L of MeOH/0.1% formic acid. 50 µL of sample was transferred to a silanized glass 96-well plate insert containing 50 µL ddH_2O and 10 µL of sample injected for LC-MS/MS analysis.

3.2.6 LC-MS/MS

Docetaxel and paclitaxel (internal standard) were separated on a Waters XSelect CSH Phenyl-Hexyl column (2.1 x 50 mm, 130 Å pore size, 5 □m particle size) using a gradient mobile phase consisting of 0.1% formic acid in water (mobile phase A) and 0.1% formic acid and 10% isopropanol in acetonitrile (mobile phase B) on a Shimadzu LC-20AD liquid chromatography system. The flow rate was 0.33 mL/min and the total run time was 6 minutes. The compounds were measured using a Thermo TSQ Ultra triple quadrupole mass spectrometer equipped with a heated electrospray ionization source in the positive ion mode. The discharge current was held at 3.7 kV and the vaporizer temperature at 225°C. Docetaxel and paclitaxel were detected by selected-reaction monitoring (SRM) using the transitions 808 -> 527 and 854 -> 286, respectively. Calibration curves were fit using linear regression with $1/X^2$ weighting in Xcalibur® v. 2.0 (Thermo Fisher Scientific, Waltham, MA).

3.2.7 Maximum Tolerated Dose Determination

The maximum tolerated doses (MTD) of free docetaxel and the docetaxel NPs were determined for a weekly x 6 schedule in female nude mice. At time of the first dose, mice were 6 weeks in age. Mice were monitored for body weight loss and overall health. Mice were sacrificed if body weight loss exceeded 20% or if they exhibited excessive signs of toxicity. The MTD was selected as the dose that did not cause excessive toxicity that required a mouse to be sacrificed or body weight loss greater than 10%.

3.2.8 Tumor Growth Inhibition Studies

16 days after cell inoculation to the lung, mice were randomized into four groups (N=8 mice per group for mice receiving free docetaxel, 9%-NP, or 20%-NP and N=6 mice per group for mice receiving saline). Mice were dosed via tail vein at 10 µL per gram body weight. Mice either received saline, 10 mg/kg docetaxel for free docetaxel, or 15 mg/kg docetaxel for mice receiving 9%-NP and 20%-NP. Mice were sacrificed when they had excessive body weight loss or excessive toxicity. Mice were imaged once a week using an IVIS Lumina Imager. Prior to imaging, mice were injected 10 µL per gram body weight with a 15 mg/mL luciferase solution. Mice were anesthetized with isoflurane prior to imaging.

3.2.9 Hematological Tests

50 µL of blood was collected into EDTA-coated tubes by submandibular bleeding the day of the first injection, 4 days after the 1st injection and 4 days after the 6th injection. Blood was analyzed for complete blood counts with differential using Heska's blood counter.

3.2.10 Statistical and Pharmacokinetic Analysis

GraphPad Prism was used to perform statistical tests. Student's t-test was utilized when only two groups were compared. One way analysis of variance (ANOVA) followed by a modified t-test for multiple comparisons was used when more than 2 groups were compared. Survival data was analyzed by Log-Rank test. Pharmacokinetic data was analyzed by noncompartmental methods using WinNonlin Professional Edition version 5.2.1 (Pharsight Corp, Cary, NC). The area under the concentration versus time curve from 0 to t (AUC_{0-t}) was calculated using the linear up/log down rule. Volume of distribution (V_d) and clearance (CL) were calculated using standard equations. The maximum concentration (C_{max}) and time of C_{max} (T_{max}) were determined by visual inspection of the concentration versus time curve data.

3.3 Results

3.3.1 Particle Characteristics

To achieve different loadings, PLA/PLGA particles were fabricated with different amounts of docetaxel. Despite having different drug loadings of docetaxel, all other particle characteristics were identical as shown in Table 3.1. As measured by dynamic light scattering (DLS), both sets of 80x320 NPs were 216 nm in hydrodynamic diameter with polydispersity indices (PDI) of less than 0.1. The total percent drug released after 24 hours was similar for both NPs (Figure 3.1F), but the 20%-NP had slightly faster burst release within the first 6 hours compared to the 9%-NP.

3.3.2 Pharmacokinetics

The pharmacokinetic parameters and profiles of the 9%-NP and 20%-NP are shown in Table 3.2 and Figure 3.1A-E. The sum total (encapsulated and released) docetaxel was

measured and is reported.

Docetaxel plasma exposure as measured by AUC of the concentration – time curve was 1.15-fold higher for mice receiving 9%-NPs compared to 20%-NPs. The V_d and CL of docetaxel was lower for the 9%-NP group. The C_{max} observed in both NP groups were not statistically significant and $T_{1/2}$ were similar. Docetaxel was not detectable at 168 hours post injection for both NPs.

Large differences in tissue docetaxel accumulation were observed between both NP groups. Mice receiving 9%-NP had 1.39-fold higher tumor docetaxel exposure than mice receiving 20%-NP. Maximum tumor docetaxel concentrations were not statistically significant between the two NP groups, but the C_{max} was observed at different times. For the 20%-NP group, the C_{max} was observed immediately after injection at 5 minutes, where as the C_{max} of the 9%-NP group was observed at 24 hours post injection.

Liver exposure of the 20%-NP group was ~1.40-fold higher than the 9%-NP group, but the observed C_{max} of both groups were not statistically significant. At 6 and 72 hours post injection, the docetaxel concentration of the 20%-NP group was statistically higher than the 9%-NP group: P=0.02 at 6 hours (12,468 ± 1,512 versus 8,025 ± 2,214) and P=0.05 at 72 hours (10,464 ± 2,828 versus 5,765 ± 525). Spleen exposure of the 20%-NP group was ~1.31-fold higher than the 9%-NP group. Spleen docetaxel concentration was statistically higher for the 20%-NP group at 1 hour post injection (P=0.03, 73,061 ± 10,855 versus 31,117 ± 19,382). Lung exposure of the 20%-NP group was ~1.56-fold higher than the 9%-NP group.

3.3.3 Maximum Tolerated Dose

The maximum tolerated dose of free docetaxel and the 20%-NP was determined in female non tumor bearing nude mice following a weekly dosing schedule for 6 weeks. The MTD of free docetaxel was expected to be 13-20 mg/kg [16,17]. Poly(L-lactide) NPs containing taxanes have been shown to have a higher MTD than the free taxane formulation [18]. Thus, 20 mg/kg was selected as the starting dose for the free docetaxel group and 30 mg/kg was selected as the starting dose for the docetaxel NP group.

The MTD of free docetaxel in female non tumor bearing mice was found to be 20 mg/kg weekly for 6 weeks. 2 mice were sacrificed within the 27 mg/kg arm and 1 mouse was sacrificed in the 35 mg/kg arm for excessive toxicity. Additionally, mice in both the 27 mg/kg and 35 mg/kg free docetaxel arms had body weight loss that surpassed 10%. The MTD of the docetaxel NPs was found to be 30 mg/kg weekly for 6 weeks. At 37.5 mg/kg, 2 mice were sacrificed after the 6^{th} dose and at 45 mg/kg, all mice were sacrificed after the 6^{th} dose. Also, the mean body weight loss of mice receiving 37.5 mg/kg and 45 mg/kg exceeded 10%. The mean body weights and survival are shown in Figure 3.2 and Table 3.3, respectively.

3.3.4 White blood cell counts

White blood cell counts (WBC) were measured one week before the 1^{st} injection and 4 days after the 1^{st} and 6^{th} injection of free docetaxel or docetaxel NPs and are reported in Table 3.4. WBC counts of all groups were not statistically significant 1 week before the 1^{st} dose as measured by one-way ANOVA. Mice receiving 9%-NP or 20%-NP did not have statistically significant differences in their WBC 4 days after the 1^{st} and 6^{th} dose.

3.3.5 Tumor Growth Inhibition

Efficacy was evaluated in an orthotopic tumor model of non small cell lung cancer. Because MTDs of the docetaxel formulations were determined in non tumor bearing mice, the MTDs may be lower in mice with orthotopic lung xenografts. To avoid toxicity attributed to docetaxel, mice received doses that were half of the MTD in non-tumor bearing mice. Survival analysis by Kaplan-Meier estimate demonstrated that 9%-NP was the superior treatment ($P=0.03$ compared to free docetaxel). Mice that received 9%-NPs or 20%-NPs had minimal or no tumor growth even 150 days post cell implantation (Figure 3.3). 6/6 mice in the saline group and 6/8 mice in the free docetaxel treatment groups had tumor growth that required mice to be sacrificed.

3.4 Discussion

We studied drug loading as a parameter that affects the therapeutic efficacy, pharmacokinetics and toxicity of docetaxel. Most NP fabrication techniques are limited to drug loadings of ~10%. PRINT® has previously demonstrated the ability to make NPs with variable drug loadings. Therefore, we prepared one NP formulation to match the loading of a taxane NP that is currently in clinical development [7] and for comparison, a second NP formulation was prepared that targeted to double the loading to 20%.

There are multiple benefits of preparing NP formulations with higher drug loading. Higher drug loading is preferable because less non active excipients are used to produce the same quantity of active pharmaceutical ingredient (API) in the NP formulation. At a higher drug loading, a lower number of particles need to be manufactured to deliver an equivalent dose of API. Reducing the number of NPs that need to be manufactured can reduce

manufacturing and processing time, raw material usage, and energy needs as many NP manufacturing processes require input of mechanical energy.

From a manufacturing viewpoint, achieving the highest drug loading possible is desired, but we have demonstrated that there are benefits in using NPs with lower drug loading. Mice receiving the 9%-NPs had more favorable pharmacokinetic profile compared to mice receiving 20%-NP. Less liver and spleen accumulation as measured by AUC was observed in mice receiving 9%-NPs compared to the 20%-NPs. Though all mice in the NP arms received 15 mg/kg of docetaxel, the total dose of particles received in the 9%-NP group was ~109 mg/kg compared to only 50 mg/kg in the 20%-NP group. The higher particle dose associated with the 9%-NP formulation may have saturated the mononuclear phagocyte system (MPS) of the liver and spleen. Reduced docetaxel accumulation in the liver and spleen of mice receiving 9%-NP may account for the increased plasma and tumor docetaxel exposure relative to the 20%-NP group. Tumor docetaxel concentration increased during the first 24 hours post injection for the 9%-NP group where as the 20%-NP group reached docetaxel C_{max} immediately after injection.

Multiple preclinical studies have evaluated the effect of concurrently or pre-administering NPs on the pharmacokinetics of a second dose of NPs [19–24]. These studies demonstrated that NP clearance could be limited by the saturation of the mononuclear phagocyte system (MPS), most notably in the liver by NPs. Additionally, differences in MPS saturation were observed between liposomes and polymeric particles of different compositions and surface chemistries [21,22,24]. Similarly, increasing the number of particles injected may saturate the MPS. Future studies are planned to investigate this phenomenon in more depth. Assays

to identify the drug distribution in the cells of the MPS after administration of docetaxel NPs to mice are currently being developed.

3.5 Conclusion

To our knowledge this is the first report to demonstrate the dependence of small molecule pharmacokinetics on drug loading in a NP. This study demonstrates that NP drug loading is an important parameter that affects docetaxel pharmacokinetics and therapeutic efficacy. As variations in drug loading may alter *in vivo* performance, these findings highlight drug loading as an important consideration in the manufacturing of NPs.

3.6 REFERENCES

[1] L. Tang, T.M. Fan, L.B. Borst, J. Cheng. Synthesis and biological response of size-specific, monodisperse drug-silica nanoconjugates. ACS Nano 2003; 6: 3954-66.

[2] K.S. Chu, W. Hasan, S. Rawal, M.D. Walsh, E.M. Enlow, J.C. Luft, et al. Plasma, tumor and tissue pharmacokinetics of Docetaxel delivered via nanoparticles of different sizes and shapes in mice bearing SKOV-3 human ovarian carcinoma xenograft. Nanomedicine 2012; 1-8.

[3] V.P. Chauhan, Z. Popović, O. Chen, J. Cui, D. Fukumura, M.G. Bawendi, et al. Fluorescent nanorods and nanospheres for real-time in vivo probing of nanoparticle shape-dependent tumor penetration. Angew Chem Int Ed Engl 2011; 50: 11417-20.

[4] H. Cabral, Y. Matsumoto, K. Mizuno, Q. Chen, M. Murakami, M. Kimura, et al. Accumulation of sub-100 nm polymeric micelles in poorly permeable tumours depends on size. Nat Nanotechnol 2011; 6: 815-823.

[5] B.R. Smith, P. Kempen, D. Bouley, A. Xu, Z. Liu, N. Melosh, et al. Shape matters: intravital microscopy reveals surprising geometrical dependence for nanoparticles in tumor models of extravasation. Nano Lett 2012; 12: 3369-77.

[6] R.B. Campbell, D. Fukumura, E.B. Brown, L.M. Mazzola, Y. Izumi, R.K. Jain, et al. Cationic charge determines the distribution of liposomes between the vascular and extravascular compartments of tumors. Cancer Res 2002; 62: 6831-6.

[7] J. Hrkach, D. Von Hoff, M.M. Ali, E. Andrianova, J. Auer, T. Campbell, et al. Preclinical development and clinical translation of a PSMA-targeted docetaxel nanoparticle with a differentiated pharmacological profile. Sci Transl Med 2012; 4: 128ra39.

[8] J. Cheng, B.A. Teply, I. Sherifi, J. Sung, G. Luther, F.X. Gu, et al. Formulation of functionalized PLGA-PEG nanoparticles for in vivo targeted drug delivery. Biomaterials 2007; 28: 869-76.

[9] X. Dong, C.A. Mattingly, M.T. Tseng, M.J. Cho, Y. Liu, V.R. Adams, et al. Doxorubicin and paclitaxel-loaded lipid-based nanoparticles overcome multidrug resistance by inhibiting P-glycoprotein and depleting ATP. Cancer Res 2009; 69: 3918-26.

[10] P.G. Tardi, R.C. Gallagher, S. Johnstone, N. Harasym, M. Webb, M.B. Bally, et al. Coencapsulation of irinotecan and floxuridine into low cholesterol-containing liposomes that coordinate drug release in vivo. Biochim Biophys Acta 2007; 1768: 678-87.

[11] A. Dicko, S. Kwak, A.A. Frazier, L.D. Mayer, B.D. Liboiron. Biophysical characterization of a liposomal formulation of cytarabine and daunorubicin. Int J Pharm 2010; 391: 248-59.

[12] Y. Yu, Y. He, B.E.I. Xu, Z. He, Y. Zhang, Y.A.N. Chen, et al. Self-assembled methoxy poly(ethylene glycol)-cholesterol micelles for hydrophobic drug delivery. J Pharm Sci 2012; 102: 1-9.

[13] E.M. Enlow, J.C. Luft, M.E. Napier, J.M. DeSimone. Potent engineered PLGA nanoparticles by virtue of exceptionally high chemotherapeutic loadings. Nano Lett 2011; 11: 808-13.

[14] Development of a Novel Orthotopic Non-small Cell Lung Cancer Model and Therapeutic Benefit of 2'-(2-bromohexadecanoyl)-Docetaxel Conjugate Nanoparticles, Submitted.

[15] M.D. Walsh, S.K. Hanna, J. Sen, S. Rawal, C.B. Cabral, A.V. Yurkovetskiy, et al. Pharmacokinetics and antitumor efficacy of XMT-1001, a novel, polymeric topoisomerase I inhibitor, in mice bearing HT-29 human colon carcinoma xenografts. Clin Cancer Res 2012; 18: 2591-602.

[16] N. Desai, V. Trieu, Z. Yao, L. Louie, S. Ci, A. Yang, et al. Increased antitumor activity, intratumor paclitaxel concentrations, and endothelial cell transport of cremophor-free, albumin-bound paclitaxel, ABI-007, compared with cremophor-based paclitaxel. Clin Cancer Res 2006; 12: 1317-24.

[17] N.P. Desai, V. Trieu, L.Y. Hwang, R. Wu, P. Soon-Shiong, W.J. Gradishar. Improved effectiveness of nanoparticle albumin-bound (nab) paclitaxel versus polysorbate-based docetaxel in multiple xenografts as a function of HER2 and SPARC status. Anticancer Drugs 2008; 19: 899-909.

[18] S.C. Kim, D.W. Kim, Y.H. Shim, J.S. Bang, H.S. Oh, S. Wan Kim, et al. In vivo evaluation of polymeric micellar paclitaxel formulation: toxicity and efficacy. J Control Release 2001; 72: 191-202.

[19] J. Dave, H.M. Patel. Differentiation in hepatic and splenic phagocytic activity during reticuloendothelial blockade with cholesterol-free and cholesterol-rich liposomes. Biochim Biophys Acta 1986; 888: 184-90.

[20] A. Gabizon, D. Tzemach, L. Mak, M. Bronstein, A.T. Horowitz. Dose dependency of pharmacokinetics and therapeutic efficacy of pegylated liposomal doxorubicin (DOXIL) in murine models. J Drug Target 2002; 10: 539-48.

[21] Z. Panagi, A. Beletsi, G. Evangelatos, E. Livaniou, D.S. Ithakissios, K. Avgoustakis. Effect of dose on the biodistribution and pharmacokinetics of PLGA and PLGA-mPEG nanoparticles. Int J Pharm 2001; 221: 143-52.

[22] H.M. Patel, N.S. Tuzel, B.E. Ryman. Inhibitory effect of cholesterol on the uptake of liposomes by liver and spleen. Biochim Biophys Acta 1983; 761: 142-51.

[23] T.M. Allen, C. Hansen. Pharmacokinetics of stealth versus conventional liposomes: effect of dose. Biochim Biophys Acta 1991; 1068: 133-41.

[24] R.L. Souhami, H.M. Patel, B.E. Ryman. The effect of reticuloendothelial blockade on the blood clearance and tissue distribution of liposomes. Biochim Biophys Acta 1981; 674: 354-71.

Formulation	Size (nm)	PDI	Zeta Potential (mV)	Weight percent docetaxel
20%-NP	216 ± 2	0.07 ± 0.01	-3.36 ± 0.16	20.1 ± 1.5
9%-NP	216 ± 1	0.09 ± 0.03	-3.11 ± 0.28	9.2 ± 1.6

Table 3.1. Particle Characteristics of 9%-NP and 20%-NP.

Specimen	Parameter	Formulation	
		9%-NP	20%-NP
Plasma	AUC (ng/mL h)	95,692 (0-72 h)	82,743 (0-72 h)
	C_{max} (ng/mL)	19,583 ± 7,997	26,753 ± 5,603
	CL (mL/h/kg)	105	121
	Vd (mL/kg)	943	1278
	$T_{1/2}$ (h)	6.6	7.4
Tumor	AUC (ng/mL h)	99,586 (0-168 h)	71,848 (0-168 h)
	C_{max} (ng/mL)	1,199 ± 1,115	1038 ± 366
Liver	AUC (ng/mL h)	1,080,179 (0-168 h)	1,513,225 (0-168 h)
	C_{max} (ng/mL)	16,359 ± 11,681	19,274 ± 10,838
Spleen	AUC (ng/mL h)	5,282,385 (0-168 h)	6,934,196 (0-168 h)
	C_{max} (ng/mL)	44,294 ± 26,239	73,061 ± 10,855
Lung	AUC (ng/mL h)	165,962 (0-168 h)	258,766 (0-168 h)
	C_{max} (ng/mL)	17,218 ± 6,347	20,200 ± 2,861

Table 3.2. Docetaxel pharmacokinetic parameters of 9%-NP and 20%-NP

	Formulation	
Dose (mg/kg)	free docetaxel	Docetaxel NP
20	3/3	-
27	1/3	-
30	-	3/3
35	2/3	-
37	-	1/3
45	-	0/3

Table 3.3. Survival at each dose level for MTD study.

	Saline	Free docetaxel (10 mg/kg)	9%-NP (15 mg/kg)	20%-NP (15 mg/kg)
1 week before 1st dose	3.8 ± 1.1	4.7 ± 2.0	3.6 ± 0.8	3.7 ± 0.8
4 days after 1st dose	3.1 ± 1.1	2.2 ± 0.5	1.4 ± 0.8	1.6 ± 0.6
4 days after 6th dose	2.3 ± 0.6	1.9 ± 0.6	1.1 ± 0.3	1.0 ± 0.4

Table 3.4. White blood cell counts (10^3/μL). N=8 per group.

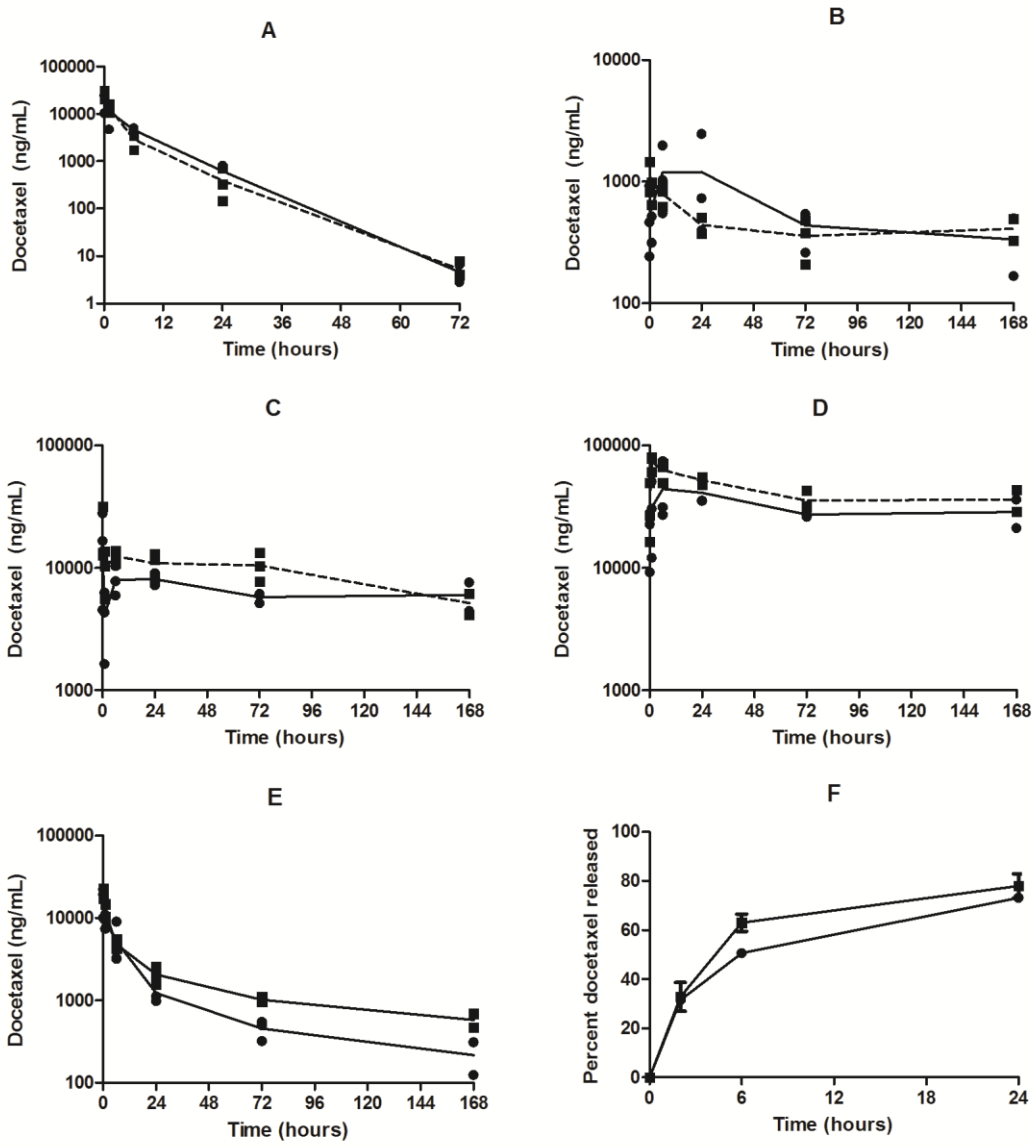

Figure 3.1. Pharmacokinetic profiles of (A) Plasma, (B) Tumor, (C) Liver, (D) Spleen and (E) Lung. (F) *In vitro* release kinetics of 9%-NP (●) and 20%-NP (■). Each replicate is shown and the lines are connected by the mean of three replicates. Mice received 10 mg/kg docetaxel.

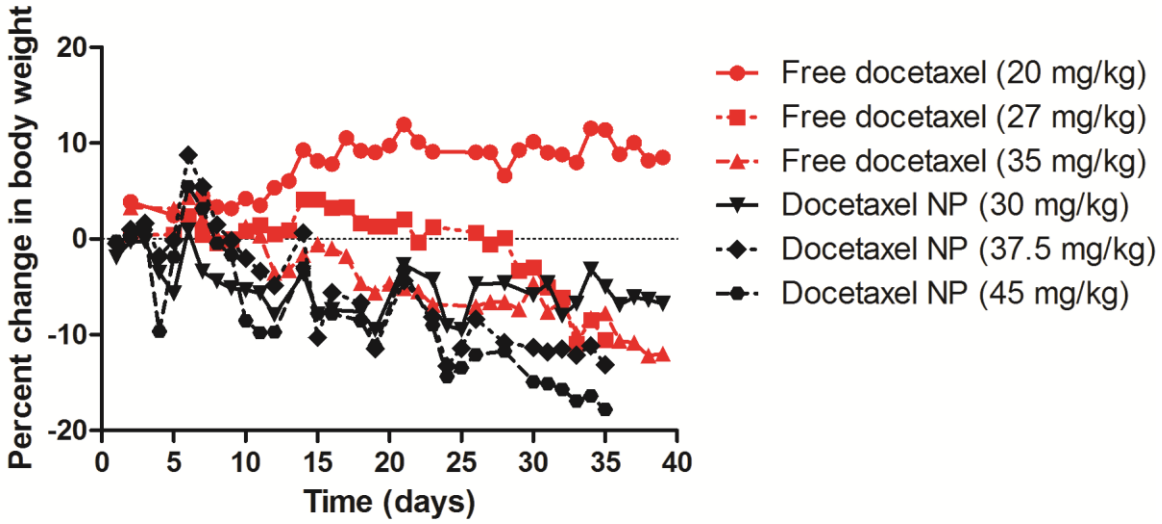

Figure 3.2. Mean body weight of mice in MTD study. Dose 1 was on Day 0. Mice were dosed weekly x 6.

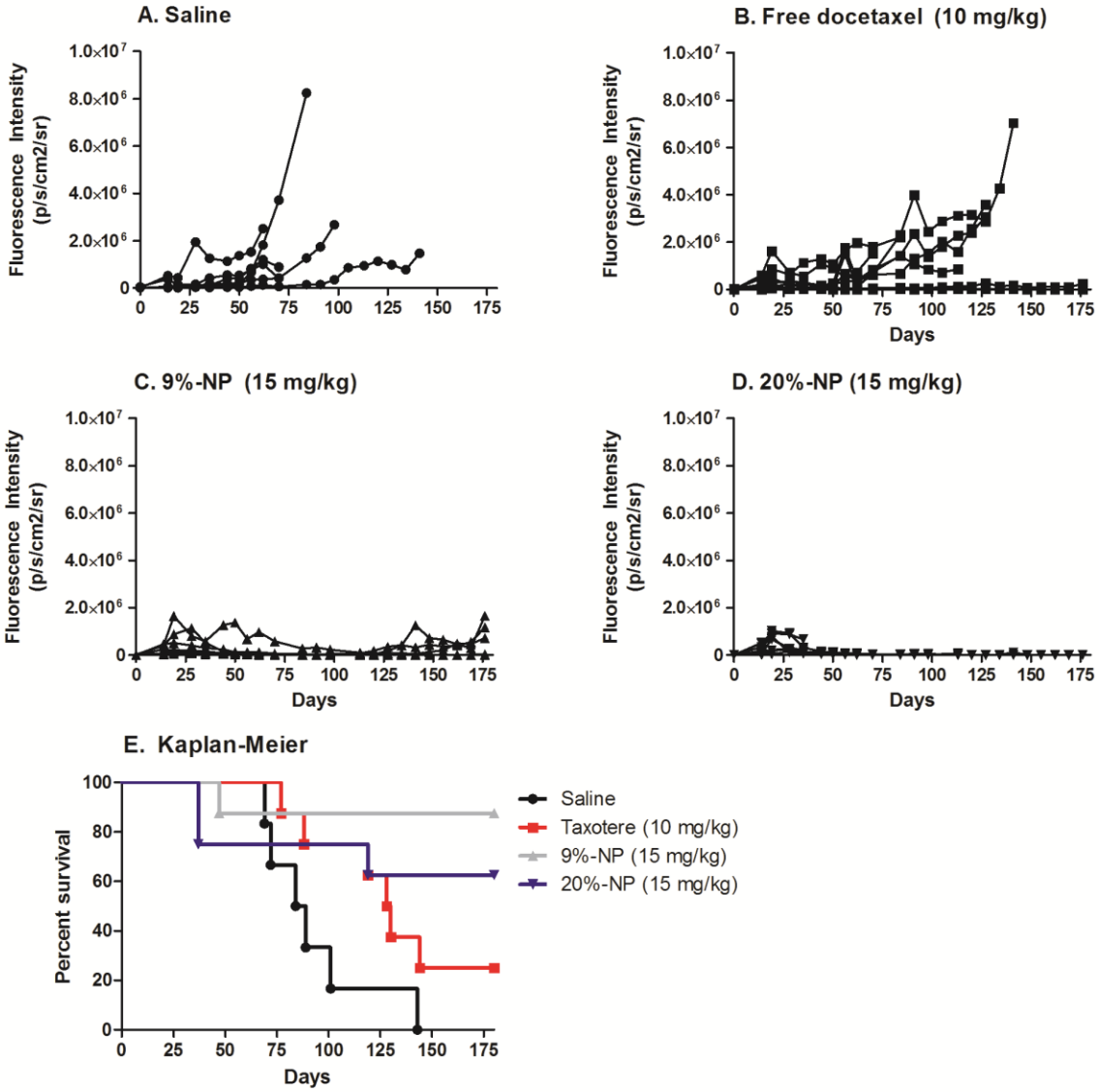

Figure 3.3. Tumor growth rates and Kaplan-Meier curve of mice with A549 orthotopic lung xenografts. Mice were dosed weekly x 6. Dose 1 was on day 16.

CHAPTER 4: REDUCED TOXICITY AND IMPROVED PHARMACOKINETIC PROFILE OF PRINT® NANOPARTICLE FORMULATIONS OF AN ACID-LABILE DOCETAXEL PRODRUG

4.1 Introduction

NP delivery of small molecule chemotherapeutic agents has the potential to improve chemotherapy delivery to solid tumors while also decreasing systemic toxicity. Sub-100 nm NPs are ideal for enhanced tumor accumulation and mononuclear phagocyte system (MPS) evasion but often have undesirable release kinetics [1–4]. As particle size decreases, surface area per unit volume increases resulting in faster release kinetics [2,5]. Furthermore, improved surface chemistries are extending particle plasma circulation times, making mechanisms for controlled release even more relevant [6]. Many approaches have been employed to prolong drug release from NPs. These strategies include the investigation of polymer composition and molecular weight [7], particle coatings [7–9], covalent attachment of drugs to nanoparticles and drug modification [10–12]. In this report, drug release rate from PLGA NPs was controlled using lipophilic acid-labile silyl ether prodrugs of docetaxel. NP release kinetics were tuned by modifying docetaxel at the C2' alcohol with silyl ether protecting groups of various alkyl chain lengths. The lipophilic acid-labile alkyl silyl ether docetaxel prodrugs were used to decrease the rate of docetaxel release from PLGA NPs with the intention of improving their *in vivo* toxicity, pharmacokinetics and efficacy. The traditional dosing regimen of taxanes is at its maximum tolerated dose (MTD) every three weeks [13,14]. Doses are administered every three weeks to allow for normal tissues to

recover, but this time period may also allow tumor cells to recover. Thus, we hypothesize that a sustained release of docetaxel will decrease the toxicity of docetaxel while enhancing its efficacy.

4.2 Materials and Methods

4.2.1 Prodrug Synthesis and Characterization

All reagents were purchased from Sigma-Aldrich, Acros Organics or Fisher Scientific and used as received unless otherwise stated. Docetaxel 99 % was used as received without any further purification from LC Laboratories. Chloro(dimethyl)octylsilane 97 % and chlorodimethylethylsilane 97 % were purchased from Sigma-Aldrich and used without any further purification. All reactions were carried out under normal atmospheric conditions at room temperature unless otherwise noted. Solvents were used as received without any further purification or drying.

NMR measurements were recorded on a Bruker AVANCE III spectrometer at room temperature. ^{1}H NMR measurements were collected at 600 MHz and ^{13}C NMR measurements were collected at 150 MHz. All chemical shifts (δ) are reported in parts per million (ppm). Electrospray ionization mass spectrometry (ESI-MS) measurements were recorded on a TriVersa Nanomate Quattro II.

4.2.2 Ethyldimethylsilyl Ether Docetaxel (C2)

In a dry 100 mL round bottom flask purged with N_2, docetaxel 99 % (1.50 g, 1.86 mmol, 1 eq.) was dissolved in anhydrous DMF (50 mL) and anhydrous pyridine (0.60 mL, 7.45 mmol, 4 eq.). Chlorodimethylethylsilane 97 % (0.23 g, 1.86 mmol, 1 eq.) was added to the solution until no more docetaxel was visualized by thin layer chromatography (TLC) (2:1 v/v hexanes:ethyl acetate; $R_f = 0.10$). After completion, the reaction was diluted with ethyl

acetate (100 mL) and washed with saturated NaCl (3 x 50 mL). The organic layer was dried over excess $MgSO_4$, filtered and the solvent removed by rotary evaporation. The product was isolated by column chromatography (silica, 2:1 v/v hexanes:ethyl acetate, R_f = 0.10), and dried *in vacuo*. Yield: 0.53 g (0.59 mmol, 31.9 %), white solid. ^{1}H NMR (600 MHz, $CDCl_3$): δ = -0.18 (s, 3H), -0.14 (s, 3H), 0.34 (m, 1H), 0.39 (m, 1H), 0.76 (t, 3H, *J* = 7.9 Hz), 1.13 (s, 3H), 1.26 (s, 3H), 1.31 (s, 9H), 1.75 (s, 3H), 1.86 (m, 1H), 1.92 (s, 3H), 2.17 (m, 1H), 2.37 (m, 1H), 2.53 (s, 3H), 2.59 (m, 1H), 3.95 (d, 1H, *J* = 7.1 Hz), 4.21 (d, 1H, *J* = 8.6 Hz), 4.26 (dd, 1H, *J* = 11.1 Hz, *J* = 6.6 Hz), 4.33 (d, 1H, *J* = 8.6 Hz), 4.46 (s, 1H), 4.98 (dd, 1H, *J* = 9.5 Hz, *J* = 1.8 Hz), 5.20 (s, 1H), 5.27 (d, 1H, *J* = 7.8 Hz), 5.53 (d, 1H, *J* = 8.6 Hz), 5.70 (d, 1H, *J* = 7.1 Hz), 6.30 (t, 1H, *J* = 8.9 Hz), 7.28 (m, 3H), 7.37 (t, 2H, *J* = 7.6 Hz), 7.49 (t, 2H, *J* = 7.7 Hz), 7.60 (t, 1H, *J* = 7.4 Hz), 8.12 (d, 2H, *J* = 7.6 Hz). ^{13}C NMR (150 MHz $CDCl_3$): δ = -3.17, -2.97, 6.33, 7.71, 9.84, 20.90, 22.81, 26.28, 28.04, 35.58, 36.52, 43.05, 46.32, 56.51, 57.45, 71.36, 71.78, 74.25, 75.09, 75.15, 76.44, 78.82, 79.63, 80.91, 84.34, 126.39, 127.57, 128.37, 128.56, 129.19, 130.07, 133.44, 135.53, 138.72, 138.99, 155.10, 166.85, 169.99, 171.41, 210.93. LR MS (m/z) observed for $C_{47}H_{63}NO_{14}Si$, $[M + H^+]^+$ = 894.33 ($[M + H^+]^+_{theoretical}$ = 894.40) and $[M + K^+]^+$ = 932.22 ($[M + K^+]^+_{theoretical}$ = 932.50).

4.2.3 Octyldimethylsilyl Ether Docetaxel (C8)

In a dry 100 mL round bottom flask purged with N_2, docetaxel 99 % (1.00 g, 1.24 mmol, 1 eq.) and imidazole (0.34 g, 4.97 mmol, 4 eq.) were dissolved in anhydrous DMF (50 mL). Chloro(dimethyl)octylsilane 97 % (0.26 g, 1.234 mmol, 1 eq.) was added to the solution until no more docetaxel was visualized by thin layer chromatography (TLC) (2:1 v/v hexanes:ethyl acetate, R_f = 0.16). After completion, the reaction was diluted with ethyl acetate (200 mL) and washed with saturated NaCl (3 x 50 mL). The organic layer was dried

over excess $MgSO_4$, filtered and the solvent removed by rotary evaporation. The product was isolated by column chromatography (silica, 2:1 v/v hexanes, ethyl acetate, R_f = 0.16), and dried *in vacuo*. Yield: 0.46 g (0.47 mmol, 37.9 %), white solid. ^{1}H NMR (600 MHz, $CDCl_3$): δ = -0.19 (s, 3H), -0.11 (s, 3H), 0.32 (m, 1H), 0.38 (m, 1H), 0.88 (t, 3H, *J* = 7.2 Hz), 1.07 (m, 2H), 1.11 (s, 3H), 1.18 – 1.31 (m, 22H), 1.72 (s, 3H), 1.85 (m, 1H), 1.91 (s, 3H), 2.17 (m, 1H), 2.35 (m, 1H), 2.53 (s, 3H), 2.56 (m, 1H), 3.94 (d, 1H, *J* = 7.0 Hz), 4.20 (d, 1H, *J* = 8.5 Hz), 4.25 (dd, 1H, *J* = 11.0 Hz, *J* = 6.7 Hz), 4.32 (d, 1H, *J* = 8.6 Hz), 4.47 (s, 1H), 4.97 (d, 1H, *J* = 9.7 Hz), 5.22 (s, 1H), 5.27 (d, 1H, *J* = 8.3 Hz), 5.57 (d, 1H, *J* = 9.1 Hz), 5.67 (d, 1H, *J* = 7.1 Hz), 6.30 (t, 1H, *J* = 8.8 Hz), 7.28 (m, 3H), 7.37 (t, 2H, *J* = 7.5 Hz), 7.48 (t, 2H, *J* = 7.7 Hz), 7.58 (t, 1H, *J* = 7.3 Hz), 8.10 (d, 2H, *J* = 7.6 Hz). ^{13}C NMR (150 MHz $CDCl_3$): δ = -2.50, -2.12, 10.02, 14.20, 14.27, 16.22, 21.18, 22.73, 22.82, 22.98, 26.42, 28.21, 29.26, 29.28, 31.97, 33.44, 35.79, 36.83, 43.22, 46.45, 56.67, 57.62, 71.48, 71.99, 74.47, 75.22, 76.66, 79.07, 79.91, 81.08, 84.40, 126.54, 127.74, 128.55, 128.78, 129.30, 130.26, 133.67, 135.61, 139.08, 139.17, 155.29, 167.12, 170.16, 171.57, 211.42. . LR MS (m/z) observed for $C_{53}H_{75}NO_{14}Si$, $[M + H^+]^+ = 978.46$ ($[M + H^+]^+_{theoretical} = 978.50$) and $[M + Na]^+ = 1000.50$ ($[M + Na^+]^+_{theoretical} = 1000.49$).

4.2.4 Nanoparticle Fabrication and Characterization

PRINT® NPs were fabricated with solutions of Poly(D,L–lactide–co-glycolide) (PLGA) and docetaxel or docetaxel prodrugs, C2 or C8, dissolved in chloroform. Unmodified docetaxel loaded into NPs is referred to as DTXL-NP whereas the prodrugs are referred to as C2-NP and C8-NP. PLGA (lactide:glycolide 85:15, 0.65 dL/g Inherent Viscosity at 30ºC) was purchased from Sigma-Aldrich. The NP fabrication and characterization follows previously published methods [15,16].

4.2.5 A549 Human Aveolar Adenocarcinoma Tumor Xenografts

All animal studies were done with an approved protocol with the University of North Carolina at Chapel Hill's Institutional Animal Care and Use Committee. All animals used were treated humanely. A549 cells were acquired from ATCC. Female nude mice, aged 4-6 weeks and ~20 grams in body weight, were acquired from the University of North Carolina at Chapel Hill's animal core. The mice were acclimated for 1 week prior to tumor cell injection. Cells (5.0×10^6 cells in 200 µL 1 x PBS) were injected subcutaneously (SC) into the right flank of each mouse. Tumor volume was calculated using the formula: tumor volume (mm^3) = (w^2 x l)/2, where w = width and l = length in mm as measured by calipers.

4.2.6 Pharmacokinetics Study

~Fourty days after cells were inoculated, mice were pair matched according to tumor volume. A median tumor size of ~150 mm^3 was targeted. All mice received 10 mg/kg docetaxel or an equivalent molar dosage of 10 mg/kg docetaxel via a single tail vein injection. Formulations were diluted to 1 mg/mL of docetaxel with saline and mice were dosed at 10 µL of solution per gram of body weight. Mice (N = 3 per time point) were sacrificed at 0.083, 1, 6, 24, 72, and 168 hours after dosing.

4.2.7 Tumor Growth Inhibition Studies

~Fourty days after cells were innoculated, mice were randomized into different treatment groups. A median tumor volume of ~150 mm^3 was targeted. Mice were dosed at 10 µL of solution per gram of body weight via tail vein injection. Dosing schedules were either weekly x 3 or weekly x 6. Doses ranged from 15 mg/kg docetaxel or docetaxel equivalents to 50 mg/kg docetaxel equivalents. Relative tumor volume (RTV) for each

mouse was calculated by dividing the tumor volume on each measured day by the tumor volume measured on day 0.

4.2.8 Hematological Tests

~50 µL of blood was collected by submandibular bleeding on the day of the 1st injection and also 4 days after the 1st and 6th injection of saline, free docetaxel or C2-NPs at 20-50 mg/kg docetaxel equivalents and collected into ethylenediaminetetraacetic acid (EDTA)-coated tubes. Blood was analyzed for complete blood counts with differential using Heska's blood counter.

4.2.9 In Vitro Conversion in Plasma

C2 and C8 were added to control CD-1 mouse K3-EDTA plasma (Bioreclamation) at 4,000 ng/mL and incubated at 37°C with shaking at 250 RPM for one week. 50 µL aliquots were removed in triplicate at 0.083, 1, 3, 6, 24, 72, and 168 hours, processed by protein precipitation and lyophilized. All samples were analyzed by LC-MS/MS on the same day.

4.2.10 In Vivo PK Analysis

Blood was harvested in K3 EDTA blood collection tubes (Fisher Scientific) and centrifuged at 2,000 x g for 5 minutes at 4°C to isolate the plasma, which was stored at -80°C. Tumors and tissues were flash frozen after harvest and stored at -80°C prior to homogenization. They were weighed and homogenized in water as previously described [15]. Pharmacokinetic data was analyzed by noncompartmental methods using WinNonlin Professional Edition version 5.2.1 (Pharsight Corp, Cary, NC). The area under the concentration versus time curve (AUC_{0-t}) from 0 to t was calculated using the linear up/log down rule. Volume of distribution (V_d) and clearance (CL) were calculated using standard

equations. The maximum concentration (C_{max}) was determined by visual inspection of the concentration versus time curve data.

4.2.11 Standard Curve and Sample Preparation

Docetaxel, C2, C8, and paclitaxel stock solutions (1 mg/mL) were stored in acetonitrile at -20°C. The standard curve concentrations of docetaxel and C2 or C8 in matrix were 1, 3, 5, 10, 30, 50, 100, 300, 500, 1000, 3000 and 5000 ng/mL and the quality control (QC) concentrations were 4, 40, 400, and 4000 ng/mL. Prodrug-only QCs were included at 400 ng/mL to monitor *ex vivo* conversion to docetaxel during sample processing. Less than 5% of C8 converted to docetaxel whereas conversion was below the limit of quantitation for C2. The matrix for the standard curve and QCs consisted of control mouse plasma for all plasma samples, or control plasma mixed 1:1 with a control tissue homogenate for the tissue being analyzed. A liver/plasma surrogate matrix was used for tumor samples. All tumor and tissue samples were mixed 1:1 with control plasma prior to analysis. Docetaxel, C2 and C8 were dissolved from the NP and extracted from 50 µL of sample by protein precipitation with 200 µL acetonitrile containing 20 ng/mL paclitaxel (internal standard). Samples were vortexed for 5 minutes and centrifuged at 3,000 x g for 10 minutes at 4°C. 140 µL supernatant was transferred to a glass 96-well plate insert containing 60 µL ddH_2O and 10 µL of sample injected for LC-MS/MS analysis.

4.2.12 LC-MS/MS

Docetaxel and C2 or C8 were separated on a Waters XSelect CSH Phenyl-Hexyl column (2.1 x 50 mm, 130 Å pore size, 5 □m particle size) using a gradient mobile phase consisting of 0.1% formic acid in water (mobile phase A) and 0.1% formic acid and 10% isopropanol in acetonitrile (mobile phase B) on a Shimadzu LC-20AD liquid chomatograph.

The flow rate was 0.33 mL/min and the total run time was 6 minutes. The compounds were measured using a Thermo TSQ Ultra triple quadrupole mass spectrometer equipped with a heated electrospray ionization source in the positive ion mode. The discharge current was held at 3.7 kV and the vaporizer temperature at 225°C. Docetaxel, C2, C8 and paclitaxel (internal standard) were detected by selected-reaction monitoring (SRM) using the transitions 808 -> 527, 894 -> 268, 978 -> 352 and 854 -> 286, respectively. Calibration curves were fit using linear regression with $1/X^2$ weighting in Xcalibur® v. 2.0 (Thermo Fisher Scientific, Waltham, MA).

4.2.13 In Vitro Cytotoxicity

The cytotoxicity of free docetaxel, C2 and C8 dissolved in DMSO was evaluated in A549 cells. Methods were previously published (16).

4.3 Results

4.3.1 Silyl Ether Docetaxel Prodrugs

The silyl ether docetaxel prodrugs, C2 and C8, were prepared by a single step reaction of docetaxel with chlorodimethylethylsilane or chloro(dimethyl)octylsilane, respectfully (Scheme 1). It has been well documented that the C2' alcohol of taxanes preferentially react with electrophiles, such as acid chlorides and anhydrides [12,17,18]. As expected, the C2' monosubstituted silyl ether prodrugs of docetaxel formed and were isolated in good yield.

The rate of conversion of the prodrug to docetaxel is the consequence of simple hydrolysis and can be tuned by altering the substituents on the silicon atom. To achieve rapid prodrug hydrolysis upon release from the NP, alkyl dimethyl silyl chlorides were selected (Figure 4.2A and 4.2B). The conversion of the prodrugs to docetaxel was studied in

mouse plasma and quantified by LC-MS/MS. The $t_{1/2}$ of C2 and C8 in mouse plasma were similar, 8 hours for the C2 prodrug and 10 hours for the C8 prodrug. The majority of the C2 and C8 prodrugs are converted within the first 24 hours. The toxicity of C2 and C8 were compared to free docetaxel *in vitro* in A549 cells (Figure 4.2C). With a 24 hour incubation time, the toxicity of the C2 and C8 prodrugs were less than that of free docetaxel.

4.3.2 Particle Characterization

Cylindrical particles with diameter (d) = 80 nm and height (h) = 320 nm were prepared using a poly(lactide-co-glycolide) polymer. By dynamic light scattering (DLS), the hydrodynamic radius was measured as ~200 nm. The particle samples were monodisperse with a polydispersity index (PDI) of less than 0.1 and as low as 0.05. PRINT® NPs were loaded with drug at weight percents of 20% - 22%. NP formulations of docetaxel and two docetaxel prodrugs, C2 and C8, were prepared. All formulations were similar in particle size and drug loading (Table 4.1). The release kinetics of the three formulations, DTXL-NP, C2-NP and C8-NP, were evaluated at 37°C in phosphate buffered saline (Figure 4.2D). The release kinetics were dependent upon the length of the alkyl chain of the docetaxel prodrug. Unmodified docetaxel was fully released after 24 hours where as the C2 prodrug was fully released after 4 days and C8 prodrug was fully released after 7 days.

4.3.3 Pharmacokinetics

The pharmacokinetic parameters and profiles of the NP formulations compared to free docetaxel at equal-molar dosing are shown in Figure 4.3 and Table 4.2. All NP formulations (prodrug + released docetaxel) had much higher plasma exposures compared to free docetaxel when measured by the AUC. A 60-fold increase in AUC was realized for the DTXL-NP where as the C2-NP and C8-NP formulations displayed a 182-fold and 84-fold

increase in AUC, respectfully. Additionally, the C2-NP and C8-NP formulations had at least 2-fold increased plasma exposure than the DXTL-NP as measured by AUC. The C_{max} of the NP formulations were many-fold higher than free docetaxel. The order of C_{max} from least to highest for the NP formulations emulated the *in vitro* release kinetics: docetaxel, C2 and then C8. However, minimal conversion of C2 and C8 to docetaxel was observed in plasma; of the total drug, the percentage of released docetaxel were 2.3% and 1.9% for C2 and C8, respectively. As expected, the CL and the V_d of the C2-NP and C8-NP as well as the DTXL-NP were much lower than free docetaxel. The C2-NP and C8-NP formulations also had decreased CL and V_d compared to the DTXL-NP.

The tumor AUC of total drug for all NP formulations were lower than that of free docetaxel. Interestingly, the extent of prodrug conversion was greater in tumor than in plasma, spleen and liver. The percentage of released docetaxel was 32% for C2 and 27% for C8. No correlation was observed between total tumor exposure and plasma exposure. Free docetaxel gave the highest tumor total drug exposure and the C2-NP gave the lowest total tumor drug exposure.

Total spleen and liver drug exposure was correlated with plasma exposure. All particle formulations had much higher exposure in spleen and liver than free docetaxel. The C2-NP formulation had the highest total plasma exposure and also the highest spleen and liver exposure.

4.3.4 Tumor Growth Inhibition and Body Weights

The efficacy of the NP formulations were compared to free docetaxel in an A549 SC xenograft mouse model. Figure 4.4A shows the tumor growth curves for the fastest release formulation, DTXL-NP, compared to the slowest formulation, C8-NP, as well as free

docetaxel and saline. All mice were given an equal molar amount of docetaxel (15 mg/kg) or an equivalent volume of saline. The RTV of the DTXL-NP was similar to free docetaxel for the first 37 days. Mice receiving the C8-NP had no tumor growth inhibition. The tumor growth curve of C8-NP was similar to that of saline. Figure 4.4B shows the tumor growth curves for the 4 day release formulation, C2–NP, at an equal molar dose to free docetaxel (20 mg/kg) and at its MTD (50 mg/kg). The RTV of the C2-NP was found to be equal to at equimolar dosing. However, at 50 mg/kg, mice receiving the C2-NP had statistically lower mean tumor volume than mice receiving free docetaxel at 20 mg/kg. Body weights (Figure 4.4C) for saline and equimolar doses of free docetaxel and C2-NP remained stable over the course of treatment, while some body weight loss was observed for the 50 mg/kg dose of C2-NP over the course of 6 doses.

4.3.5 White Blood Cell (WBC) Counts

Table 4.3 shows the mean WBC count of mice receiving the C2-NP (20 mg/kg or 50 mg/kg) compared to free docetaxel (20 mg/kg). Blood was collected 4 days after injection and measured for complete blood counts. Mice receiving the C2-NP formulation at an equal molar dose to free docetaxel trended towards statistically higher WBC 4 days after the 1st dose and statistically higher WBC 4 days after the 6th dose.

4.4 Discussion

The implications of slower docetaxel release rates from PLGA NPs on pharmacokinetics and efficacy was investigated in an A549 model of NSCLC in mice. The PRINT® process was utilized to prepare monodisperse particles with identical docetaxel loading. Alkyl silyl ether prodrugs of docetaxel were synthesized and formulated into NPs to achieve variable release rates while maintaining the same particle composition (Table 1).

These prodrugs were ideal to study the effect of release rate on *in vivo* toxicity, pharmacokinetics and efficacy because release kinetics could be tuned by varying the alkyl chain length, without altering prodrug conversion kinetics. The rate of prodrug conversion is controlled by the steric hindrance of the substituents on the silicon atom. Rapid conversion was observed for both the C2 and C8 prodrugs (Figure 4.2A and B), because dimethyl substituents were selected. A previous study that utilized a diisopropyl constituent yielded no conversion over 168h (data not shown).

In vitro release kinetics (Figure 4.2D) confirmed that release rates of the prodrugs were much slower than that of unmodified docetaxel. The PK parameters also suggest a slower release with higher exposures of the prodrug in plasma, liver and spleen. The exposure in tumor was greater for Taxotere and DTXL-NP for the time course observed in this study. Silyl ethers are widely used as protecting groups in synthetic organic chemistry and can be easily removed by acid hydrolysis [19]. Thus, conversion of the C2 and C8 prodrugs should occur faster in the acidic environment of the tumor than in the plasma and tissues, and subsequently minimize systemic toxicity. Preferential conversion of the silyl ether prodrugs in the tumor was observed in the PK studies. The percentage of released docetaxel in the plasma for the C2-NP and C8-NP was 2.3% and 1.9%, but 32% and 27% within the tumor. The extent of conversion of C2 and C8 prodrugs to docetaxel observed in the liver and spleen were also much less than the conversion observed in the tumor. The docetaxel prodrugs, C2 and C8, reduce cytotoxicity (Figure 4.2C) and systemic toxicity (as evidenced by stable body weights), by decreasing drug release while the particles are in circulation and also by preferentially converting in the acidic environment of the tumor.

The benefit of using the C2-NP was realized in the WBC measurements. At equal molar doses to free docetaxel, mice receiving the C2-NP had statistically higher WBC than free docetaxel. Structure-activity relationship studies of taxanes reported in the literature have demonstrated that modification of the C2' alcohol greatly diminishes the activity of taxanes [20]. In addition to the sustained release of C2-NP formulation, the diminished activity of the C2 prodrug in the C2-NP formulation may also contribute to its reduced neutropenic effect. In clinical studies that compared administration of docetaxel once every 3 weeks [75 mg/m^2] versus once a week [33.3 mg/m^2], patients receiving weekly administrations of docetaxel had less toxicity, including less neutropenia and leucopenia [21]. Furthermore, dosing schedule was not found to alter overall survival. Increasing the duration of dose administration, as achieved by deceasing drug release rate from NPs, may explain the observed reduction in hematological toxicity. In addition to achieving reduced toxicity, a sustained release formulation is more convenient for patients over a cycle of chemotherapy.

Interestingly, despite greatly reducing systemic toxicity, the C2-NP was equal in effectiveness to free docetaxel at equal molar dose in an A549 xenograft mouse model. Sustained released of docetaxel from a NP may not improve the efficacy of docetaxel, but may improve the safety profile and improve patient convenience. However, because of the observed improvement in the safety profile of the C2-NP, a much higher dose of docetaxel was delivered. This translated to an equivalent docetaxel dose of 50 mg/kg, which resulted in improved tumor growth inhibition compared to free docetaxel at 20 mg/kg.

4.5 Conclusions

PRINT® technology was used to prepare particles of the exact same size and composition to study the effect of sustained drug release on *in vivo* toxicity, pharmacokinetics and efficacy. The use of an acid-labile docetaxel prodrug, C2, that reduces drug release rate from PLGA NPs and preferentially converts within the tumor greatly increased plasma exposure, decreased systemic toxicity while also improving tumor growth inhibition. The silyl ether prodrug strategy is amenable to many other chemotherapeutics and may have wide implications in improving the pharmacokinetics and safety profile of small molecule chemotherapeutics when delivered via a NP.

4.6 REFERENCES

[1] H. Cabral, Y. Matsumoto, K. Mizuno, Q. Chen, M. Murakami, M. Kimura, et al. Accumulation of sub-100 nm polymeric micelles in poorly permeable tumours depends on size, Nat Nanotechnol 2011; 6: 815-823.

[2] Y.-H. Lee, F. Mei, M.-Y. Bai, S. Zhao, D.-R. Chen. Release profile characteristics of biodegradable-polymer-coated drug particles fabricated by dual-capillary electrospray. J Control Release 2010; 145: 58-65.

[3] S.D. Perrault, C. Walkey, T. Jennings, H.C. Fischer, W.C.W. Chan. Mediating tumor targeting efficiency of nanoparticles through design. Nano Lett 2009; 9: 1909-15.

[4] L. Tang, T.M. Fan, L.B. Borst, J. Cheng. Synthesis and biological response of size-specific, monodisperse drug-silica nanoconjugates. ACS Nano 2012; 6: 3954-66.

[5] A. Budhian, S.J. Siegel, K.I. Winey. Controlling the in vitro release profiles for a system of haloperidol-loaded PLGA nanoparticles. Int J Pharm 2008; 346: 151-9.

[6] M.E.R. O'Brien, N. Wigler, M. Inbar, R. Rosso, E. Grischke, A. Santoro, et al. Reduced cardiotoxicity and comparable efficacy in a phase III trial of pegylated liposomal doxorubicin HCl (CAELYX/Doxil) versus conventional doxorubicin for first-line treatment of metastatic breast cancer. Ann Oncol 2004; 15: 440-9.

[7] X. Luan, R. Bodmeier. Influence of the poly(lactide-co-glycolide) type on the leuprolide release from in situ forming microparticle systems. J Control Release 2006; 110: 266-72.

[8] R.C. Smith, M. Riollano, A. Leung, P.T. Hammond. Layer-by-layer platform technology for small-molecule delivery. Angew Chem Int Ed Engl 2009; 48: 8974-7.

[9] K.C. Wood, J.Q. Boedicker, D.M. Lynn, P.T. Hammond. Tunable drug release from hydrolytically degradable layer-by-layer thin films. Langmuir 2005; 21: 1603-9.

[10] M.C. Parrott, M. Finniss, J.C. Luft, A. Pandya, A. Gullapalli, M.E. Napier, et al. Incorporation and controlled release of silyl ether prodrugs from PRINT nanoparticles. J Am Chem Soc 2012; 134: 7978-82.

[11] S.M. Ansell, S.A. Johnstone, P.G. Tardi, L. Lo, S. Xie, Y. Shu, et al. Modulating the therapeutic activity of nanoparticle delivered paclitaxel by manipulating the hydrophobicity of prodrug conjugates. J Med Chem 2008; 51: 3288-96.

[12] L. Feng, H. Wu, P. Ma, R.J. Mumper, S.R. Benhabbou. Development and optimization of oil-filled lipid nanoparticles containing docetaxel conjugates designed to control the drug release rate in vitro and in vivo. Int J Nanomedicine 2011; 6: 2545-56.

[13] F.V. Fossella, R. DeVore, R.N. Kerr, J. Crawford, R.R. Natale, F. Dunphy, et al. Randomized phase III trial of docetaxel versus vinorelbine or ifosfamide in patients with advanced non-small-cell lung cancer previously treated with platinum-containing chemotherapy regimens. The TAX 320 Non-Small Cell Lung Cancer Study Group. J Clin Oncol 2000; 18: 2354-62.

[14] M. Martin, T. Pienkowski, J. Mackey, M. Pawlicki, J.-P. Guastalla, C. Weaver, et al. Adjuvant docetaxel for node-positive breast cancer. N Engl J Med 2005; 352: 2302-13.

[15] K.S. Chu, W. Hasan, S. Rawal, M.D. Walsh, E.M. Enlow, J.C. Luft, et al. Plasma, tumor and tissue pharmacokinetics of Docetaxel delivered via nanoparticles of different sizes and shapes in mice bearing SKOV-3 human ovarian carcinoma xenograft. Nanomedicine 2012; 1-8.

[16] E.M. Enlow, J.C. Luft, M.E. Napier, J.M. DeSimone. Potent engineered PLGA nanoparticles by virtue of exceptionally high chemotherapeutic loadings. Nano Lett 2011; 11: 808-13.

[17] S. Ali, I. Ahmad, A. Peters, G. Masters, S. Minchey, A. Janoff, et al. Hydrolyzable hydrophobic taxanes: synthesis and anti-cancer activities. Anticancer Drugs 2001; 12: 117-28.

[18] L. Huynh, J.-C. Leroux, C. Allen. Enhancement of docetaxel solubility via conjugation of formulation-compatible moieties. Org Biomol Chem 2009; 7: 3437-46.

[19] T. Greene, P. Wuts. Greene's Protective Groups in Organic Synthesis, 4th Edition, 2007.

[20] D.G.I. Kingston. Taxol, a molecule for all seasons. Chem Commun 2001; 867-880.

[21] C. Gridelli, C. Gallo, M.D. Maio, E. Barletta, A. Illiano, P Maione, et al. A randomised clinical trial of two docetaxel regimens (weekly vs 3 week) in the second-line treatment of non-small-cell lung cancer. The DISTAL 01 study. Br J Cancer 2004; 91: 1996-2004.

Formulation	Size (nm)	PDI	Zeta Potential (mV)	Weight percent loading
DTXL-NP	213 +/- 1	0.07 +/- 0.01	-2.81 +/- 0.23	21.2 +/- 0.5
C2-NP	205 +/- 2	0.05 +/- 0.02	-2.65 +/- 0.52	20.7 +/- 0.4
C8-NP	208 +/- 7	0.09 +/- 0.02	-3.78 +/- 0.36	22.3 +/- 1.9

Table 4.1. NP Characterization of DTXL-NP, C2-NP and C8-NP Formulations.

Specimen	Parameter	Formulation					
		Taxotere	DTXL-NP	C2-NP		C8-NP	
		DTXL	DTXL	C2	DTXL	C8	DTXL
Plasma	AUC (ng/mL h)	1,227	79,192	227,735	5,381	103,979	2,003
	C_{max} (ng/mL)	2,314	23,359	78,952	1,994	83,785	1,678
	CL (mL/h/kg)	8,150	126	49	1,858	96	4,992
	Vd (mL/kg)	10,508	4513	237	9,535	1,171	85,924
Tumor	AUC (ng/mL h)	73,222	60,858	26,799	12,897	40,611	15,056
	C_{max} (ng/mL)	453	476	946	288	573	127
Liver	AUC (ng/mL h)	7,246	73,270	131,023	19,916	142,440	9,840
	C_{max} (ng/mL)	12,254	6,693	23,359	12,637	16,108	2,566
Spleen	AUC (ng/mL h)	30,162	390,222	1,004,965	28,442	468,037	28,442
	C_{max} (ng/mL)	6,391	20,580	64,365	2,419	77,983	5,261

Table 4.2. Pharmacokinetic parameters of free docetaxel, DTXL-NP, C2-NP and C8-NP Formulations.

Time Point	Saline	Free docetaxel (20 mg/kg)	C2-NP (20 mg/kg)	C2-NP (50 mg/kg)
	WBC (10^3 cells/μL)			
Day of dose 1	2.07 +/- 0.21	1.34 +/- 0.36	1.67 +/- 0.54	1.54 +/- 0.35
4 days after dose 1	2.81 +/- 0.91	0.84 +/- 0.65	*1.41 +/- 0.65	0.49 +/- 0.38
4 days after dose 6	3.43 +/- 1.13	1.53 +/- 0.52	†3.00 +/- 1.10	0.56 +/- 0.28

Table 4.3. White blood cell counts measured 4 days after injection with Saline, free docetaxel or C2-NP at two dose levels. * indicates trend towards statistically significance compared to free docetaxel (P=0.12). † indicates statistical significance compared to to free docetaxel (P=0.008).

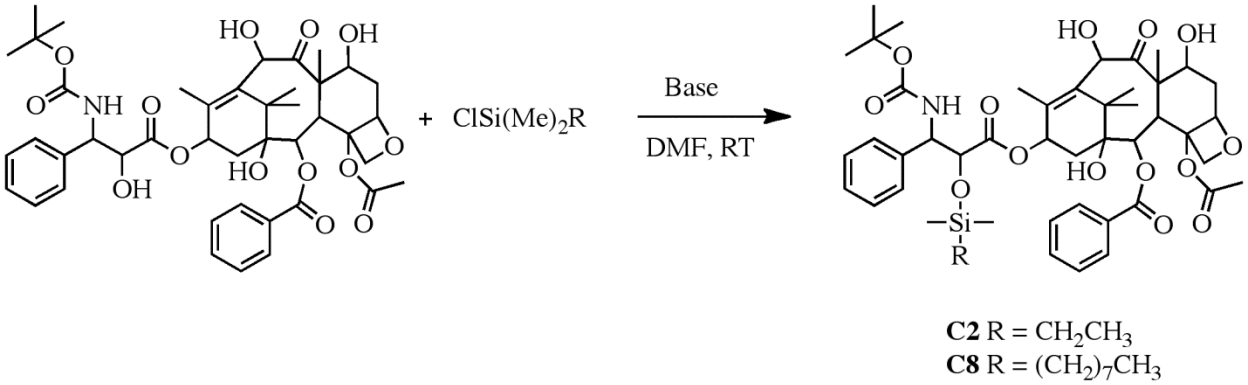

Figure 4.1. Synthesis of Silyl Ether Docetaxel Prodrugs

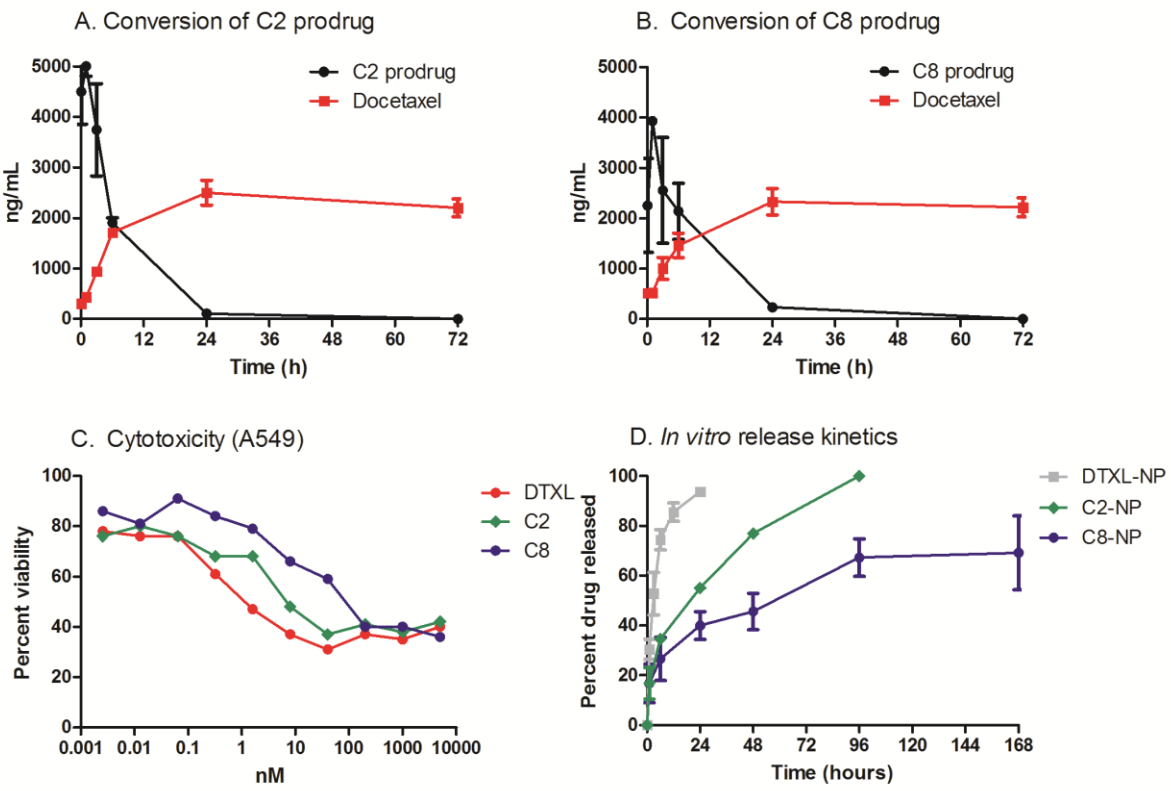

Figure 4.2. A. Release kinetics of docetaxel, C2 and C8 from PLGA NPs in PBS at 37ºC. B. Cytotoxicity of docetaxel, C2 and C8 on A549 cells *in vitro*. C. Hydrolysis of C2 in plasma. D. Hydrolysis of C8 in plasma.

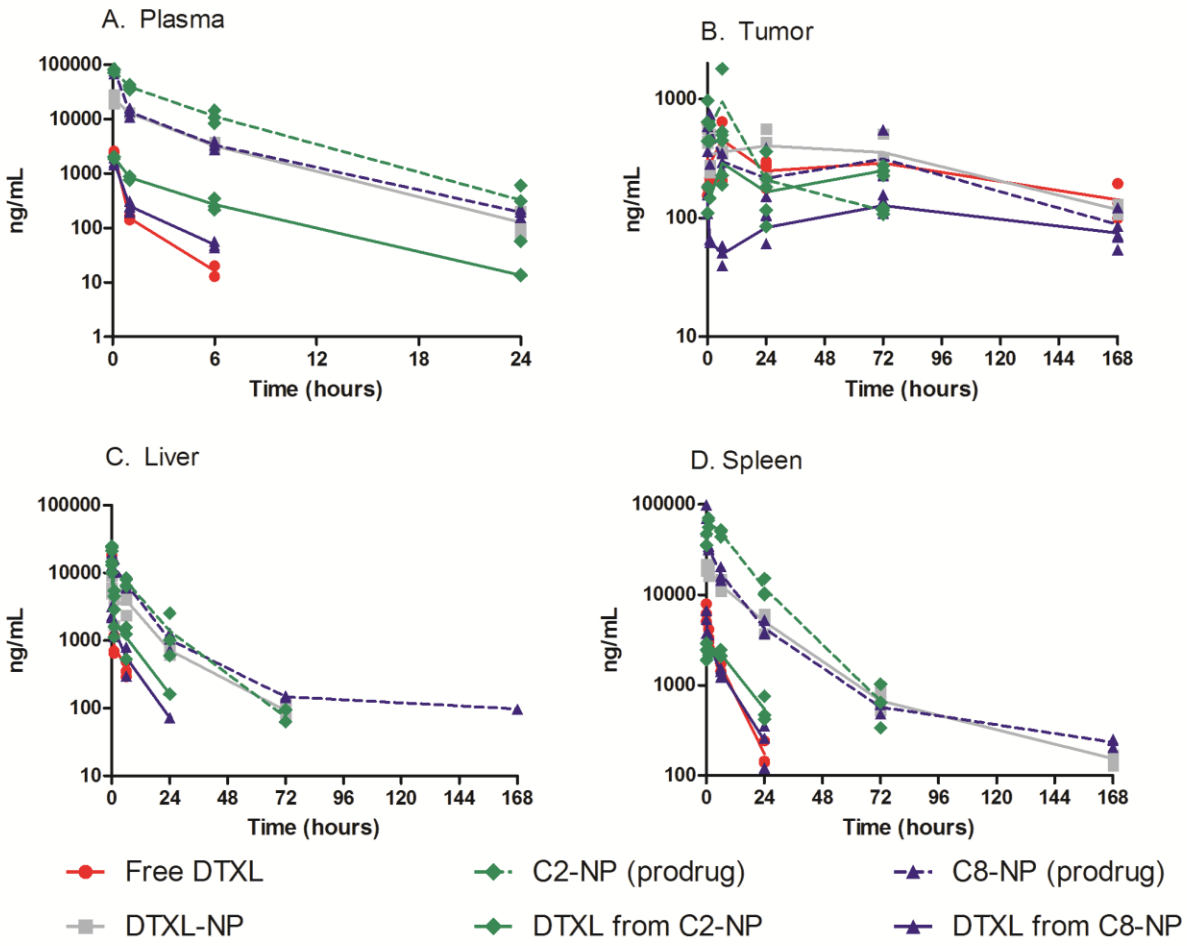

Figure 4.3. Pharmacokinetic profiles of free docetaxel, DTXL-NP, C2-NP and C8-NP Formulations. Each replicate is shown and lines are connected by the means of three replicates at each time point. Mice received 10 mg/kg docetaxel or docetaxel equivalents.

A. Efficacy of C8-NP

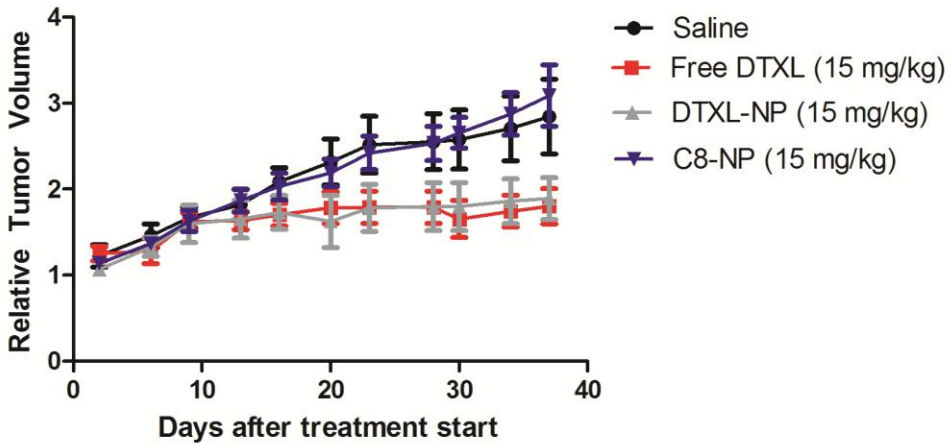

B. Efficacy of C2-NP

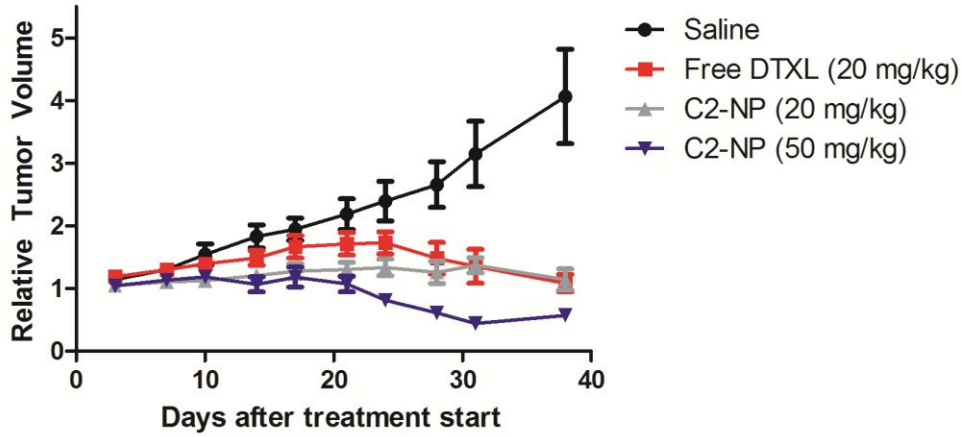

C. Body weight

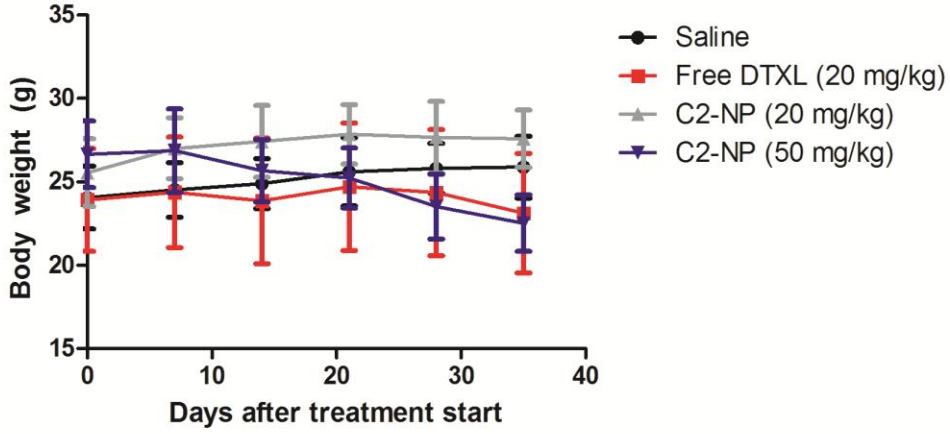

Figure 4.4. A-B.Tumor growth inhibition curves (Mean±SEM). Mice received 3 or 6 weekly doses. Mice receiving C2 NP at 50 mg/kg had tumor volumes lower than mice receiving free docetaxel ($P<0.05$ starting on day 10). C. Body weights (Mean±Std Dev).

CHAPTER 5: CONCLUSIONS AND FUTURE DIRECTIONS

Nanoparticle delivery of chemotherapeutics has the potential to significantly alter small molecule pharmacokinetics, and thus change its efficacy and toxicity. The brief review (Chapter 1) of the various particle technologies that have been used reformulate taxanes demonstrates that different particle types yield vastly different pharmacokinetics, efficacy and toxicity of the encapsulated small molecule. In this dissertation, the nanoparticle fabrication platform PRINT® was utilized to produce particles with well controlled geometry and composition to evaluate how key characteristics such as particle size of rod-shaped particles, drug loading and release kinetics affect *in vivo* performance.

Nanoparticles are useful as drug delivery carriers for oncology because they limit distribution to normal tissues, but passively target solid tumors by extravasation through leaky vasculature. To improve plasma exposure and extravasation of nanoparticles to the tumor, design has focused on optimizing surface chemistry and particle size of spherical particles. Thus, the focus of this research was to explore how the formulation parameters: particle size of rod-shaped particles, drug loading and release kinetics can affect chemotherapeutic delivery. Decreased particle diameter, drug loading and release kinetics were all found to improve the sum total pharmacokinetics of docetaxel with varying effects on efficacy and toxicity.

Multiple groups have demonstrated that reduced particle size of spherical particles has lead to improved tumor accumulation and penetration *in vivo* [1-4], but high aspect ratio

rod-shaped particles have not been as thoroughly characterized *in vivo*. Rod-shaped particles may be advantageous because recent studies have shown that cationic [5] or targeted [6] high aspect ratio particles improve cellular uptake in cancer cells. However, improving particle internalization *in vitro* through use of a rod-shaped particle design may decrease the particles' potential for passive targeting to tumors. Particle size greater than 200 nm may increase particle clearance by the spleen [7], so rod shaped particles could potentially have increased clearance compared to spherical particles commonly used for oncology which are ~100 nm in diameter. Docetaxel encapsulated in high aspect ratio 80x320 nm particles had favorable sum total plasma docetaxel pharmacokinetics *in vivo* in a SKOV-3 subcutaneous xenograft model. Mice receiving 80x320 nm docetaxel particles had less docetaxel exposure within their liver and spleen, but higher docetaxel exposure in the tumor (0-24 h) compared to mice receiving 200x200 nm particles. The smaller dimension of a particle appeared to have a greater influence on biodistribution than its longer dimension, which is favorable for high aspect ratio particles. However, in this study, sum total docetaxel was monitored, rather than the particle or the polymer itself. Thus, future studies will track the particle itself to confirm the findings concluded by tracking sum total drug. Additionally, future studies will compare cylindrical particles with similar diameter to 80 nm, but with shorter length than 320 nm. If cylindrical particles with a common diameter, but different lengths have similar biodistribution, then high aspect particles may be the preferred particle for delivering chemotherapeutics by improving cellular uptake without compromising passive tumor accumulation.

Drug loading was also evaluated as a parameter to alter sum total docetaxel pharmacokinetics. For a given dose of drug, changing the nanoparticle drug loading varies

the number of particles or mass of polymer within that dose. Because nanoparticles are primarily cleared by the MPS, changing the number of particles injected may alter nanoparticle clearance if the MPS can be saturated. Decreased drug loading, which increases the number of particles injected per mass drug dosed, increased the sum total plasma exposure and decreased the sum total spleen and liver exposure of docetaxel. As a result, the lower drug loading nanoparticle dose had increased sum total docetaxel exposure and trend towards improved efficacy.

Future studies will evaluate a wider range of drug loadings at the same docetaxel dose to confirm that sum total docetaxel plasma exposure increases nonlinearly as drug loading decreases. Gabizon et al. demonstrated that plasma and tumor doxorubicin concentrations from Doxil increased disproportionally as dose increased [7]. In addition, doxorubicin concentrations within the liver did not increase proportionally with increased dosage [7]. Gabizon et al. hypothesized that Doxil clearance was saturated, which resulted in nonlinear pharmacokinetics as dosage was increased. Thus, it may be possible for the rate of clearance for docetaxel encapsulated in a nanoparticle to be decreased as drug loading is lowered

Though it is unknown whether or not the rate of clearance is affected in humans as dosage of a nanoparticle is changed, the results of chapter 3 demonstrate that particles of different drug loadings were not bioequivalent in a preclinical model. Thus, during nanoparticle development, keeping nanoparticle drug loading a consistent parameter is important to achieve consistent results. Additionally, drug loading and even dosing regimen may be important parameters to control to maximize efficacy achieved by nanoparticle formulations through increasing sum total plasma drug exposure. Interestingly, though sum

total plasma drug exposure was increased with lower drug loading, toxicity was measured by white blood cell counts were not statistically different for the formulations tested.

Finally, the results of chapter 4 demonstrated that controlling drug release rate with a prodrug strategy had significant impact on the toxicity and efficacy of docetaxel. A slower release rate through use of a prodrug also increased the sum total drug plasma exposure. However, too slow of a release, as seen with the C8 prodrug, did not result in any efficacy. For a non targeted nanoparticle, efficacy is caused by a combination of drug released from the nanoparticle within the plasma and drug that is released from the nanoparticle at the site of the tumor. A potential explanation is that a slow release rate may not achieve efficacy because the minimum effective concentration in the plasma was not reached. If the prodrug is retained too long within the particle, the majority of the prodrug docetaxel would be cleared while still encapsulated in the particle. As a result, even though sum total prodrug docetaxel is high within the plasma, the drug is not available to exert its pharmacological activity unless released. Alternatively, the particle could be reaching the tumor, but at the site of the tumor, the drug is still releasing too slowly to kill tumor cells at a rate greater than tumor growth.

However, with a moderate release rate provided by the C2 prodrug, similar efficacy compared to free docetaxel was observed at equal molar dosing. In addition, toxicity was improved compared to free docetaxel; the MTD of C2-NP was 2.5-times higher than free docetaxel compared to only 1.5-times higher for the regular DTXL-NP. This improved tolerability a much higher dose of C2-NP to be administered relative to free docetaxel to achieve improved tumor growth inhibition. The toxicity profile of docetaxel was likely improved by minimizing the percent of free docetaxel released from the C2-NP. Thus, future

work will further explore the relationship between the AUC of released docetaxel and toxicity as well as efficacy. Potentially, the pharmacokinetic parameters of the released drug molecule may be a better predictor of toxicity and efficacy.

The work of this dissertation has demonstrated that controlling key nanoparticle formulation parameters drastically varies the pharmacokinetics of the encapsulated docetaxel or docetaxel prodrug to alter toxicity and efficacy. By selecting the optimal parameter for each formulation variable, improved nanoparticle formulations can ultimately be designed to achieve the maximum improvement in tolerability and efficacy of the encapsulated chemotherapeutic. Decreased particle diameter and drug loading may decrease drug clearance to maximize plasma AUC to improve tumor accumulation, but sustained release may manage toxicity by controlling the pharmacokinetics of the released chemotherapeutic.

5.1 REFERENCES

[1] F. Yuan, M. Dellian, D. Fukumura, M. Leunig, D.A. Berk et al. Vascular Permeability in a Human Tumor Xenograft: Molecular Size Dependence and Cutoff Size. Cancer Res 1995; 55: 3752-56.

[2] H. Cabral, Y. Matsumoto, K. Mizuno, Q. Chen, M. Murakami et al. Accumulation of sub-100 nm polymeric micelles in poorly permeable tumors depends on size. Nat Nanotechnol 2011; 12: 815-23.

[3] L. Tang, N.P. Gabrielson, F.M. Uckun, T.M. Fan, J. Cheng. Size-dependent tumor penetration and in vivo efficacy of monodisperse drug-silica nanoconjugates. Mol Pharm 2013; 10: 883-92.

[4] L. Tang, T.M. Fan, L.B. Borst, J. Cheng. Synthesis and biological response of size-specific, monodisperse drug-silica nanoconjugates. ACS Nano 2012; 6: 3954-66.

[5] Gratton SE, Ropp PA, Pohlhaus PD, Luft JC, Madden VJ, Napier ME, et al., The effect of particle design on cellular internalization pathways. Proc Natl Acad Sci USA 2008; 105: 11613-8.

[6] Barua S, Yoo JW, Kolhar P, Wakankar A, Gokarn YR, Mitragotri S. Particle shape enhances specificity of antibody-displaying nanoparticles. Proc Natl Acad Sci USA 2013; 110: 3270-5.

[7] Moghimi SM, Hunter AC, Murray JC. Long-circulating and target-specific nanoparticles: theory to practice. Pharmacol Rev 2001; 53: 283-318.